UNIVERSIDADE DE LISBOA
FACULDADE DE CIÊNCIAS
DEPARTAMENTO DE FÍSICA

Cholesteric liquid crystals confined in toroidal droplets

Ana Regina Azevedo da Luz Fialho

Dissertação

Mestrado em Física
(Área de Especialização: Física da Matéria Condensada e Nanomateriais)

Orientação: Professora Doutora Margarida Telo da Gama e Doutor Nuno M. Silvestre

2015

Acknowledgements

First of all, I would like to thank my thesis supervisors Margarida Telo da Gama and Nuno M. Silvestre, and the Principal Investigator of the project that led to the development of this thesis, Nelson R. Bernardino, for all the help and guidance they have given me during the development of this work. I am grateful for their patience and for all the discussions and insightful comments. I also acknowledge the support from the Portuguese Foundation for Science and Technology (FCT) through grants PTDC/FIS/119162/2010, EXCL/FIS-NAN/0083/2012, SFRH/BPD/63183/2009(NRB), and SFRH/BPD/40327/2007(NMS), which have made this study possible.

I would also like to thank my colleagues, and Carolina Figueirinhas Pereira in particular, for their companionship and for the fresh and unbiased views that they have shared about my work.

I have also benefited from interesting and useful discussions with many people that I met during conferences and poster presentations, and for that I am thankful.

Finally, I would like to thank my family and friends for supporting me unconditionally during the course of these years.

"*Liquid crystals are beautiful and mysterious; I am fond of them for both reasons.*"

Pierre Gilles de Gennes, Nobel Prize Laureate

Abstract

The great potential of nematics and cholesterics for optical applications is indisputable. Liquid crystal displays (LCDs) have dominated the flat display industry for over 50 years and are still of standard use in small everyday devices. In a common LCD cell, the liquid crystal is confined in between two flat glass plates. However, the confinement of liquid crystals inside curved geometries leads to more exotic structures, with applications ranging from bio-sensors to optical switches and privacy windows.

The ground state of a liquid crystal enclosed into curved droplets is the result of the competition between the elasticity and the topological constraints imposed by the confinement. Depending on the geometry of the droplet, the minimal energy configurations may exhibit singularities in the orientation - topological defects - as imposed by the Poincaré-Hopf theorem. Recent techniques allow for the controlled production of droplets with non-spherical geometries, like single and multiple torii. For the toroidal geometry, configurations with no defects are permitted. It is the ideal system for the study of curvature effects on the liquid crystal alignment.

In this thesis, we perform the numerical study of the cholesteric configurations inside a toroidal droplet. We model the system on the mesoscale, using the Landau-de Gennes free energy. We aim to understand how the curvature affects the twist and the formation of cholesteric layers inside toroidal droplets. We perform the study in three stages, analysing different curved geometries, to isolate the curvature effects.

Our results show that the stresses introduced by the curvature influence the orientation and cause distortions in the natural periodicity of the cholesteric. These distortions depend on the radius of curvature and on the commensurability between the pitch and the dimensions of the system. The effect causes a symmetry breaking in the position of the cholesteric layers inside the toroidal droplet.

Keywords: Cholesteric, Confinement, Topological constraints, Toroidal droplet, Landau-de Gennes Modelling

Resumo

Nemáticos e colestéricos são conhecidos pelas suas aplicações ópticas. O grande potencial destes materiais tem origem na ordem dos seus constituintes. Nas fases nemática e colestérica, as moléculas são livres de se movimentar no espaço, tal como num líquido convencional, mas obedecem a uma ordem orientacional de longo alcance. A orientação das moléculas define uma direção preferencial, quebrando a isotropia do espaço. Desta forma, nemáticos e colestéricos são na realidade líquidos anisotrópicos.

A diferença entre as duas fases é que o colestérico é constituído por moléculas quirais. Enquanto as moléculas num nemático tendem a estar homogeneamente alinhadas em todo o espaço, a quiralidade do colestérico favorece uma torção espontânea. Num colestérico livre de constrangimentos, as moléculas tendem a torcer ao longo de uma direção, descrevendo uma hélice no espaço. O comprimento que corresponde a uma volta de 2π na orientação das moléculas define a periodicidade do colestérico e tem o nome de pitch.

Como consequência da ordem orientacional das moléculas, as propriedades elásticas, electromagnéticas e ópticas do material são também anisotrópicas. Estas propriedades macroscópicas assentam num meio que é fluido e flexível. Assim, nemáticos e colestéricos são extremamente sensíveis a estímulos externos e tornam-se ideais para aplicações tecnológicas controláveis. A realização deste conjunto de propriedades esteve na base do desenvolvimento dos ecrãs de cristal líquido (LCDs).

Os ecrãs LCD dominaram o mercado dos mostradores planos durante mais de 50 anos e são ainda de uso padrão em pequenos aparelhos do quotidiano. A geometria de uma célula LCD comum é, de facto, bastante simples e consiste num cristal líquido confinado entre duas placas planas de vidro. Contudo, o confinamento de cristais líquidos no interior de superfícies curvas conduz a estruturas mais exóticas, com aplicações que vão desde bio-sensores a interruptores ópticos e janelas de privacidade.

Assim, após o grande triunfo da tecnologia de ecrãs planos, os investigadores estão agora interessados no papel de geometrias confinantes mais complexas nas propriedades dos cristais líquidos. Devido aos constrangimentos topológicos, as superfícies curvas revestem-se de um interesse especial. O estado fundamental de um cristal líquido confinado no interior de gotas curvas é o resultado da competição entre a elasticidade e os constrangimentos topológicos impostos pelo confinamento.

Dependendo da geometria da gota, as configurações de energia mínima podem exibir singularidades na sua orientação, designadas por defeitos topológicos. Esta é uma consequência de um importante teorema em topologia, o teorema de Poincaré-Hopf, para superfícies com característica de Euler diferente de zero.

Estudos efectuados em gotas e camadas esféricas de cristal líquido mostram que os defeitos podem promover interações direcionais entre partículas, sendo estas apontadas como possíveis unidades para a construção de metamateriais com propriedades de auto-agregação. As propriedades materiais do cristal líquido, o ancoramento à superfície e as características geométricas do sistema, todos funcionam como parâmetros de controlo na estabilidade das configurações. Assim, é possível controlar o número e posição dos defeitos, com o objectivo de arquitetar diferentes estruturas alvo.

De forma a complementar a investigação da influência da topologia nas propriedades físicas dos cristais líquidos, é importante estudar sistemas com geometrias distintas da esférica. Em experiências recentes, foi possível ultrapassar as limitações impostas pela tensão superficial e produzir gotas com géneros diferentes de zero, tal como o toro.

O toro tem característica de Euler igual a zero. Desta forma, a configuração na superfície do toro não necessita de incluir defeitos topológicos. Contudo, a curvatura influencia as configurações do cristal líquido de forma não trivial. Em gotas toroidais de nemático, uma estrutura quiral com torção ao longo do toro é observada.

Nesta tese, considerámos uma gota toroidal preenchida com cristal líquido colestérico. A periodicidade do colestérico define uma escala de comprimento adicional, aumentando a complexidade do sistema. O nosso objectivo é a compreensão de como a razão entre o pitch do colestérico e os raios do toro afectam as configurações. Também, e de um ponto de vista mais fundamental, queremos compreender como é que o confinamento e curvatura do sistema irão afectar a periodicidade intrínseca do colestérico. Devido à sua característica de Euler, a forma toroidal é distinta de outras formas curvas e permite estas estudos fundamentais sem a presença de defeitos topológicos.

Começamos, no Capítulo 1, por motivar o presente estudo, e posiciona-lo no quadro de investigação atual. Uma breve história da descoberta dos cristais líquidos é apresentada. É dado especial enfâse às incomuns propriedades dos cristais líquidos que deixaram perplexos os cientistas da época e os levaram a concluir que tinham de estar perante um novo estado da matéria. De seguida, as diferentes fases de cristal líquido são classificadas. A caracterização de nemáticos e colestéricos é alvo de maior atenção. O Capítulo 1 termina com uma revisão bibliográfica dos avanços científicos

no que diz respeito à área de cristais líquidos confinados por superfícies curvas. A interface com a topologia e as possíveis aplicações tecnológicas são realçadas.

No Capítulo 2, é introduzida a teoria necessária para modelar o cristal líquido colestérico. Apresentamos a argumentação que leva à construção de um parâmetro de ordem tensorial. De seguida, mostramos como é que a energia livre que descreve as simetrias do sistema à escala mesoscópia pode ser obtida como um funcional do parâmetro de ordem definido. Este modelo é designado por modelo de Landau-de Gennes e inclui contribuições provenientes da ordem do sistema e da sua elasticidade efetiva. A energia que descreve a interação com superfícies é também abordada. Por fim, introduzimos o conceito de defeitos topológicos e a formulação do teorema de Poincaré-Hopf, discutindo as suas implicações para diferentes tipos de superfícies curvas.

No Capítulo 3, descrevemos de forma breve os métodos numéricos utilizados para obter as configurações de equilíbrio do cristal líquido colestérico. Deduzimos um sistema de equações diferenciais que nos permite assumir simetria cilíndrica no sistema. Assim, é possível realizar os cálculos numéricos apenas numa secção transversal bidimensional. Por fim, discutimos as vantagens e desvantagens das nossas técnicas numéricas para a minimização da energia livre em sistemas com e sem simetria cilíndrica.

Os resultados numéricos são apresentados no Capítulo 4. Este Capítulo está dividido em três partes, cada uma correspondente a um diferente sistema curvo. O desenvolvimento do estudo com recurso a três diferentes níveis de complexidade tem o objectivo de isolar os efeitos da curvatura no colestérico. Começamos por considerar um sistema simples que consiste apenas num colestérico junto a uma parede curva. De seguida consideramos toros com e sem imposição de simetria cilíndrica.

Os nossos resultados mostram que as tensões introduzidas pela curvatura influenciam a orientação do colestérico junto à superfície. Este efeito propaga-se a toda a configuração, causando distorções na periodicidade natural do colestérico. As distorções são tanto mais intensas quanto menor o raio de curvatura.

As consequências deste efeito refletem-se nas estruturas toroidais. No interior do toro, a orientação das moléculas torce ao longo da direção radial, formando camadas colestéricas nesta direção. No limite de curvatura nula, que corresponde a um cilindro infinito, estas camadas são concêntricas. Quando a curvatura é introduzida, há uma quebra de simetria na posição das camadas colestéricas. Mais uma vez, verifica-se que o efeito é mais acentuado nas geometrias com menor raio de curvatura. Aqui, a comensurabilidade entre o pitch e as dimensões do sistema, em

particular o raio da secção transversal do toro, tem também um papel importante. Sistemas em que as dimensões são comensuráveis são mais estáveis e apresentam texturas mais simétricas.

Palavras-Chave: Colestérico, Confinamento, Constrangimentos topológicos, Gota toroidal, Modelo de Landau-de Gennes

Contents

1 Introduction **1**

2 Mesoscopic Modeling **10**
2.1 Order Parameter 10
2.2 Landau-de Gennes Model 13
2.2.1 The nematic-isotropic transition 13
2.2.2 Elastic energy 17
2.3 Surface anchoring 20
2.4 Topological Defects 22

3 Numerical Methods **27**
3.1 Systems with cylindrical symmetry 28
3.2 Systems without cylindrical symmetry 31
3.3 Visualization technique 32

4 Cholesteric Confined by Curved Surfaces **34**
4.1 Cholesteric close to a curved wall 35
4.2 Toroidal droplet with imposed axial symmetry 42
4.3 Toroidal droplet with planar degenerate anchoring 46

5 Conclusions **50**

A The Euler-Lagrange equations **53**

B Euler-Lagrange equations with cylindrical symmetry **56**

C The twist parameter **59**

List of Figures

1.1 The nematic, smectic and columnar phases. 3
1.2 The schlieren texture. 4
1.3 The cholesteric phase. 5
1.4 The twisted nematic display. 6
1.5 Three types of thin nematic shells with variable number of defects. . . 7
1.6 Experimental technique for stabilizing toroidal droplets. 8

2.1 Schematic representation of the molecular orientation in a nematic phase. 11
2.2 Nematic alignment for rod-like and disk-like molecules. Distinction between positive and negative scalar order parameter. 15
2.3 Typical profiles of the Landau-de Genes free energy for different temperature regimes. 16
2.4 Schematic representation of the three basic elastic deformation modes: splay, twist and bend. 17
2.5 Schematic representation of the director field for configurations with topological defects. 23
2.6 Representation of singular and non-singular disclination lines in cholesteric liquid crystals. 24
2.7 Packing of hexagonal cells in a flat space, and on the surface of a sphere. 25
2.8 Alignment of rod-like particles on flat and spherical surfaces. 26
2.9 Alignment of rod-like particles on a toroidal surface. Axial and twisted configurations. 26

3.1 Schematic representation of the curved systems generated by considering rectangular and circular cells with imposed cylindrical symmetry around the z axis. 31
3.2 Visualization of the equilibrium cholesteric configurations with the Paraview software. 33

4.1 The toroidal shape defined by the two curvature radii. 35
4.2 Schematic representation of the three-dimensional system simulated in Section 3.1. 36
4.3 Initial conditions for the system studied in Section 3.1. 37
4.4 Comparison of the equilibrium configurations for the rectangular cell systems with and without curvature. $P_0 = 1000\xi$. 38
4.5 Equilibrium configurations for rectangular cell systems with a natural pitch $P_0 = 500\xi$ and curvature radius $R = 1\xi$. 40
4.6 Variation of $\frac{P}{P_0}$ with the distance to the symmetry axis for different values of the curvature radius. 41
4.7 Cholesteric configurations for rectangular cell systems with fixed boundary conditions of director perpendicular to the symmetry axis. 41
4.8 Equilibrium configurations for a cholesteric liquid crystal inside an infinite cylinder with radius $r = 500\xi$. 43
4.9 Comparison between the cholesteric configurations for the no curvature limit and for a curvature radius $R = 50\xi$. 44
4.10 Cholesteric configurations for a system with radius of curvature $R = 50\xi$. 45
4.11 Equilibrium configurations for a toroidal droplet with planar degenerate anchoring on the surface. 47
4.12 Surface configurations of a cholesteric inside a toroidal droplet with increasing natural pitch P_0, approaching the nematic limit. 48
4.13 Configurations of a cholesteric inside a torus, with multiple layers. . . 49
4.14 Orientation of the director field on the surface of a torus filled with cholesteric liquid crystal. 49

Chapter 1

Introduction

The beginning of liquid crystal science dates back to 1888, when the Austrian botanist Friedrich Reinitzer reported his studies on the melting behaviour of cholesteryl benzoate, a cholesterol based compound [1]. He found that the substance did not melt as other materials. Instead, he described it as having two melting points. At 145.5C the solid crystal melted into a cloudy liquid, and at 178.5C the cloudiness suddenly disappeared, giving way to a clear transparent liquid [2].

Reinitzer sought help from Dr. Otto Lehmann, a well-known German crystallographer, to interpret his findings. Lehmann had developed a heating stage microscope that allowed him to observe in detail the crystallization process as he slowly lowered the temperature of the samples [3]. Together, the two scientists were able to discredit the claims that the unusual behaviour were due to anomalies in the crystallization process or to the presence of impurities. They had found a fourth state of matter.

The new phase displayed a unique kind of order, intermediate between crystalline and liquid-like ordering. It shared properties of the two states. It flowed like a liquid, but, like a crystal, it also gave rise to optical patterns when observed under polarized light. These materials were first called *soft crystals*. A succession of designations followed, including *floating crystals* and *crystalline fluids*. Finally, Lehmann coined the term *liquid crystal* in order to stress the combination between the flow properties of a liquid and the optical properties of a crystal [3].

The unusual macroscopic properties of liquid crystals are a result of the microscopic ordering of its constituents. In a crystal, the molecular constituents are regularly stacked on a three-dimensional periodic lattice. This results in a long range positional order. In addition, if the molecules are non-spherical, there is also a long range orientational order of the molecular axes. Both kinds of order are lost in the

transition to the conventional liquid. In a liquid, there is only short range order in the positions of the molecular centres of mass. The molecules are free to move around, having no fixed position or orientation. Let us designate this kind of liquid by isotropic liquid, in order to avoid any ambiguity.

Some materials, however, do not transition from the solid to the liquid phase directly. Instead, they have a sequence of transitions, passing through intermediate phases (mesophases). The term liquid crystal designates a class of mesophases characterized by having a long range orientational order, while the positional order is completely, or at least partially, absent [4]. Liquid crystals are more ordered than a conventional, or isotropic, liquid but less ordered than a crystal.

The order in the orientation of the molecules is the common property to all liquid crystal phases. To generate such an alignment, the molecular building blocks must be anisotropic, either elongated or disk-like [5]. The orientational order emerges from the alignment of the molecules which, in turn, arises from the packing of their anisotropic shapes.

The degree of positional order that is present, distinguishes between different liquid crystal phases. The three types of liquid crystal phase are the nematic, the smectic, and the columnar phase [5]. A nematic has no positional order. It corresponds to a liquid but, because the molecules are orientationally ordered, defining a preferred direction, it is an anisotropic liquid (see Fig. 1.1 (a) and (b)). A smectic has unidimensional positional order in three dimensions. The system can be perceived as a set of two-dimensional layers of liquid, separated by a well defined distance (see Fig. 1.1 (c)). Columnar phases have two-dimensional order in three dimensions. They can be described as a two-dimensional array of columns of liquid (see Fig. 1.1 (d)).

Liquid crystals can still be classified in thermotropic and lyotropic, according to the parameter that induces the phase transitions [4]. For thermotropic liquid crystals temperature is the fundamental thermodynamic control parameter determining the phase. Lyotropic liquid crystals form only in a solution, upon the addition of a solvent. The controlling parameter driving the transition between phases is, in this case, the concentration of the liquid crystal molecules.

The nematic is the simplest liquid crystal phase. In a nematic, the molecules move in space with three translational degrees of freedom, just like in a liquid. However, the molecular orientations tend to align with each other, pointing, on average, along the same direction. The orientation of the molecules defines a preferred direction, destroying the space isotropy that characterizes conventional liquids.

The anisotropy of the nematic medium affects its macroscopic properties. Mea-

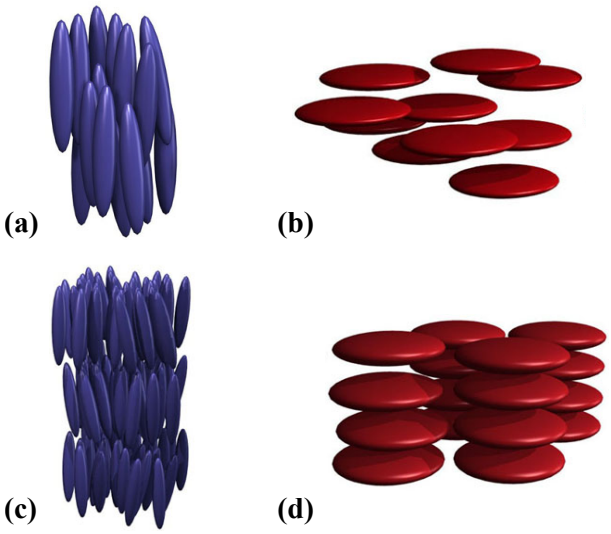

Figure 1.1: (a) Nematic ordering for rod-like molecules. (b) Nematic ordering for disk-like molecules. (c) Smectic phase. (d) Discotic columnar phase. Figure reproduced from [6].

surements of the elastic, electric, magnetic, optical and flowing properties of a nematic give different results depending on the direction along which they are measured [5]. These anisotropic properties are carried by a fluid flexible medium. Nematics are, therefore, extremely sensitive to external perturbations, making them ideal for controllable technological applications.

Nematics are also affected by the interaction with confining surfaces. The contact with a surface imposes a preferred orientation of the molecules at the surface. This orientation can be controlled by the chemical treatment of the surface.

The interaction with surfaces and external fields might frustrate the otherwise uniformly aligned state of the nematic, imposing deformations of the orientation. Smooth deformations are called elastic deformations because they trigger an elastic restoring response. However, it is not always possible for the molecular orientational field to adjust to any external conditions by distorting smoothly everywhere in the sample. In this case, the orientational field exhibits singularities, *i.e.* regions of undefined direction. These regions are called topological defects. In nematics, both point and line defects (formally called disclinations) are observed [7]. In a defect region, the order of the material is disrupted. The presence of defects has a large influence in the physical properties of the material. Understanding their behaviour and interactions is, therefore, crucial to the exploitation and control of material properties. Because of their orientational order and their flexibility, nematics are the ideal system for the study of the topological defects.

Defects can be easily detected in a nematic, when viewed under crossed polarizers. Point defects appear as black brushes, called *schlieren* brushes, and disclination lines as black threads [4]. The black regions are a consequence of the optical extinction that occurs when the alignment of the molecules has different direction than the polarization vector. In this case there is no transmission of light. Knowing the orientation of the molecules at the black regions allows one to infer the presence of the topological defects. A typical nematic texture, called schlieren texture, is shown in Fig. 1.2. It exhibits regions with brushes and threads resulting from point defects and disclination lines respectively.

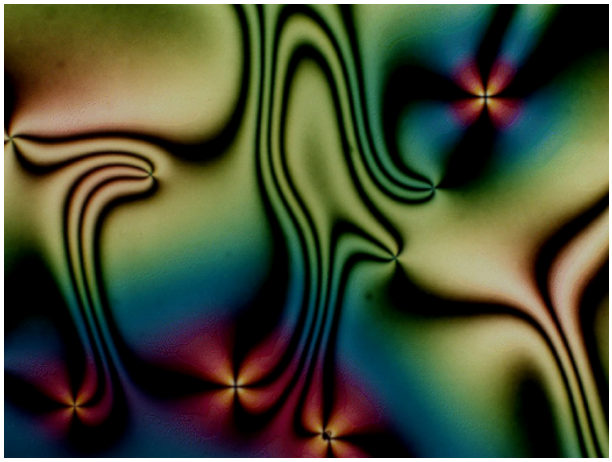

Figure 1.2: The schlieren texture. Nematic observed under crossed polarizers. The black brushes correspond to topological point defects. Microphotograph courtesy of Oleg D. Lavrentovich, Liquid Crystal Institute, Kent State University.

When chiral molecules, *i.e.* molecules with no mirror symmetry plane, are added to the nematic phase, the chirality expresses itself by favouring a periodic twist of the orientation in the direction perpendicular to the molecular axes (see Fig. 1.3 (a)). The resultant phase receives the name of cholesteric, or chiral nematic. The molecular orientation in the cholesteric phase describes an helical shape. The distance for which the orientation of the molecules rotates by 2π is the periodicity of the cholesteric and it is called the cholesteric pitch (see Fig. 1.3 (b)).

The pitch of the cholesteric is usually of the order of a few hundred nanometres. Because of their periodic structure, cholesterics give rise to visible light Bragg scattering. Cholesterics are therefore ideal for optical applications. On the other hand, the pitch is also very sensitive to temperature, pressure, chemistry, etc. Since the change of these conditions provokes a change of color of the material, cholesterics make for very accurate sensors.

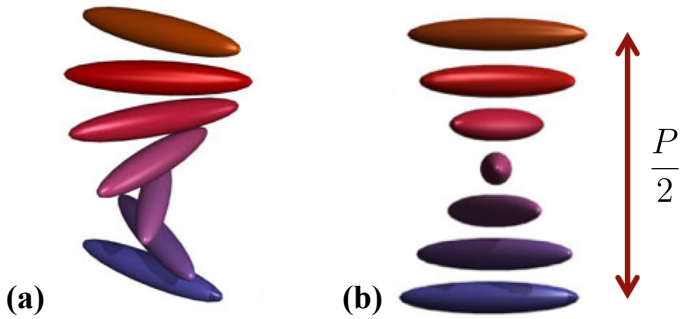

Figure 1.3: The cholesteric phase. (a) Molecular orientation twisting in space in a cholesteric phase. (b) The molecular orientation twists with a periodicity designated by pitch P. The pitch is the distance over which the orientation twists by a complete 2π turn. A π turn corresponds to half a pitch $\frac{P}{2}$. Figure reproduced from [6].

Although their great potential for optical applications is nowadays widely recognised, the study of liquid crystals remained solely of academic interest until 1962 [8]. The first use of a nematic in a display device changed this picture. The Liquid Crystal Display (LCD) technology revolutionized the display industry. Cathode ray tube displays gave way to flat panels and new smaller devices, such as laptops, tablet computers and smartphones, were made possible.

The first, and simplest, model of a liquid crystal display is known as the twisted nematic (TN) display. The TN display is still the most commonly used for everyday items like watches and calculators [9].

The device consists of a nematic liquid crystal sandwiched between two glass plates. Each of the glass plates is treated to fix the orientation of the nematic on its surface. The orientation at the top is perpendicular to the orientation at the bottom. In between the top and bottom plates, the nematic assumes a twisted configuration (see Fig. 1.4 (a)). This structure is similar to the cholesteric state, and sometimes a small amount of a chiral material is added to ensure a uniform twist. A polarizer is put outside each of the glass plates so that the direction of polarization matches the direction of the molecules on the glass surface. When the light passes through the cell in this twisted state, the direction of polarization is rotated in the same way as the molecular orientation. Therefore, the light reaches the bottom polarizer with a polarization parallel to it and it is transmitted. This is called the transmissive state because the cell gives a bright output. If a field is applied, with an intensity superior to the necessary threshold for the Fredericks transition [5], the molecules align with the field and the polarized light is no longer rotated (see Fig. 1.4 (a)). As a result, the light reaches the bottom polarizer with a direction perpendicular to

it, and it is not transmitted. The cell appears dark.

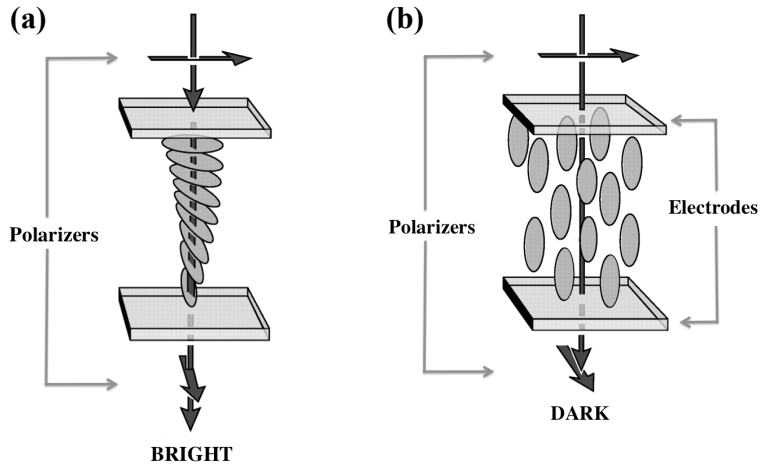

Figure 1.4: The twisted nematic display. (a) The transmissive or bright state. The configuration of the nematic in between the two glass plates is twisted. The direction of polarization of the light rotates with the orientation of the nematic, reaching the bottom polarizer parallel to it. (b) The dark state. The nematic has the orientation of the electric field. The direction of polarization of light is not rotated, and it reaches the bottom polarizer perpendicular to it. Figure reproduced from Fig. 6 of [8]

The twisted nematic display takes advantage of the nematic properties of surface anchoring, elasticity and interaction with external fields. These allow the switch between the two different configurations, alternating between the bright and dark states, to form the image. The geometry of the apparatus is relatively simple, with the nematic confined in between two flat glass plates. Regardless of its geometrical simplicity, the development of the LCD was the basis for a multi-billion dollar industry [10].

The interfacial ordering of liquid crystals continues to be a topic of research [11]. Apart from its fundamental interest, there are also potential implications to the creation of self-assembling metamaterials, and liquid crystal based responsive materials, such as bio-sensors [12].

When the confining surfaces or interfaces are curved, the number and complexity of possible configurations increases greatly, as do the parameters that allow the switching between them. For an ordered medium on a curved surface, the geometry plays an important role. The curvature itself might influence the state of alignment of the liquid crystal. The curvature imposes a strain that can be accommodated in different ways, depending on the elastic constants of the medium as well as on the elastic anisotropy [13]. On the other hand, there are the topological constraints.

There is a fundamental topological theorem, due to Poincaré and Hopf [14] that imposes the presence of topological defects depending on the topological characteristics of the surface.

Rather than being just a disturbing presence in the equilibrium configurations, the defect structures can actually be of relevance in material science and engineering, as proposed in [15]. The basic idea is to use spherical liquid crystal droplets, or colloids coated by liquid crystals, as building blocks for self-assembling materials. The liquid crystal configurations will inevitably include defects. Since defects possess different physical properties, they can be functionalized with target molecules to promote directional interactions [16]. In this sense, the number of defects acts as a valence of the particle [17]. The control of the number of defects and their positions, by geometrical or external parameters, can allow to target different architectures.

This possibility has triggered extensive experimental and computational study of the nematic configurations inside spherical nematic droplets and spherical nematic shells [18, 19]. The configurations on nematic shells have been found to depend on the boundary conditions [20, 21] and thickness of the shell [22, 23, 24, 25]. Figure 1.5 shows three types of thin nematic shells with variable number of defects. In this case, the number of defects was controlled by the thickness and thickness anisotropy of the shell.

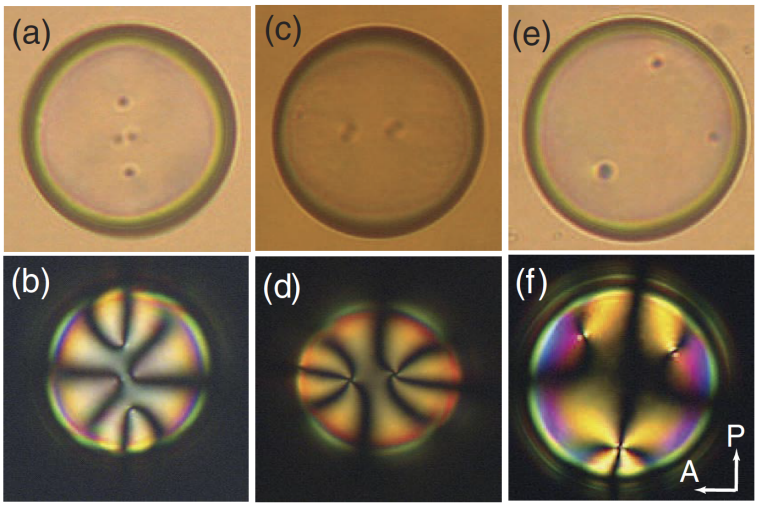

Figure 1.5: Three types of thin nematic shells commonly observed, distinguished by the number and type of defects: (a), (b) four defects; (c), (d) two defects; (e), (f), three defects. Figure reproduced from Fig. 3 of [23].

The development of novel experimental techniques has allowed the production of droplets with different topologies. In order to overcome the surface tension that favours the spherical shape of the droplets, a continuous viscous phase is used to

provide a mold [26]. With this technique, it is possible to produce toroidal droplets and droplets with multiple handles. The procedure consists of injecting the liquid crystal through a thin needle into a rotating bath that contains the viscous phase (see Fig. 1.6 (a)). The angular speed of the bath and the speed of injection of the liquid crystal define the geometrical parameters of the droplet. When the rotation completes one full turn, the process stops and the outside medium stabilizes the droplet (see Fig. 1.6 (b)).

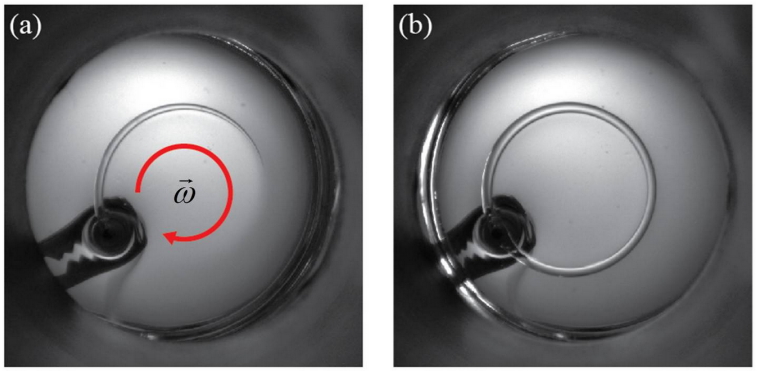

Figure 1.6: Experimental technique for stabilizing toroidal droplets. (a) Injection of the liquid crystal into the rotating viscous bath. A curved jet is formed. (b) Once the jet concludes one full revolution, the toroidal droplet is closed. Figure reproduced from Fig. 6 of [27].

Studying the behaviour of ordered media confined inside such non-trivial geometries is pivotal to understand the role of the topological constraints in the liquid crystal configurations. Also, by varying the geometry of the droplets, more textures are made available, with different optical properties and possible applications to photonic devices.

The toroidal shape has a particular topological significance. For a toroidal surface, the Poincaré-Hopf theorem allows the existence of configurations without topological defects. From a fundamental point of view, such configurations allow a deeper study of the curvature effects on the observed textures. The curvature together with the elasticity of the material induce configurations that could not be predicted just by the assumption of topological constraints [28]. This is the case of the toroidal nematic droplet, for which theoretical [29] and experimental [30] studies have found that, when a nematic is confined inside a toroidal droplet, there is a spontaneous breaking of the mirror symmetry, with a persistent chiral twisted state along the torus.

The introduction of a cholesteric liquid crystal in place of a nematic introduces

a new length scale to the problem. The intrinsic periodicity of the cholesteric, the pitch, is one extra parameter that can be adjusted to define the stability regime of each possible configuration. Also, the set of possible textures increases. This was first exemplified in the theoretical studies of cholesterics in cylindrical cavities [31, 32]. The equilibrium configurations depend on the radius of the cylinder and on the elastic constants, just like the nematic, but also on the natural pitch of the cholesteric.

Spherical cholesteric droplets have also been reported in the literature. The studies confirm that the ratio between the pitch of the cholesteric and the radius of the sphere is one of the main parameters affecting the configuration [33]. The configurations found are more diverse than the nematic ones, with an internal defect structure that is only possible due to the natural spontaneous twist of the cholesteric [34].

The main goal of this thesis is to expand the study of the confinement of cholesterics to the toroidal droplet. The topology of the cholesteric is identical to the one of the nematic. Therefore, for a cholesteric it is still possible to have configurations with no topological defects. This allows us to investigate how the curvature of the system affects the natural periodicity of the cholesteric and how the relation between the pitch and the geometrical parameters of the torus define the equilibrium configurations.

We start by introducing, in Chapter 2, the theoretical background for the modelling of the cholesteric liquid crystal. We present the tensorial order parameter and construct the free energy that describes the symmetries of the system. We also introduce the concept of topological defects and the formal statement of the Poincaré-Hopf theorem, discussing its implications for different curved surfaces.

In Chapter 3, we briefly describe the numerical methods used to obtain the equilibrium configurations of the cholesteric liquid crystal. We deduce a system of differential equations that allow us to assume cylindrical symmetry on the system and calculate only on a two-dimensional cross-section. Then, we discuss the advantages and disadvantages of our numerical techniques for the minimization of the free energy of the system.

We present our numerical results in Chapter 4. This Chapter is divided in three parts, each one corresponding to a different curved system. We use different systems to isolate the effects of curvature on the cholesteric. We find that the curvature influences the orientation of the cholesteric close to the surface. This effect propagates through the configuration and it is responsible for distorting the periodicity of the cholesteric inside the toroidal droplet.

Chapter 2

Mesoscopic Modeling

2.1 Order Parameter

The anisotropic molecules in nematic and cholesteric phases display long range orientational order. The molecules align, on average, along a common direction, described by a unit vector called *director*[4]. In nematics, the director varies in space due to external fields and constraints in the system (e.g. boundary conditions). In the case of cholesterics, the director twists spontaneously, describing an helicoidal shape. Nematics and cholesterics show a higher degree of order than the isotropic liquid [7]. To put this in a quantitative basis, it is necessary to define an order parameter that is non-zero in the liquid crystal phase and that vanishes, for symmetry reasons, in the isotropic phase.

The director $\mathbf{n}(\mathbf{r}, t)$ at position $\mathbf{r}$ and time t is defined as the ensemble average of molecular orientations $\mathbf{u}(\mathbf{r}, t)$ within a given volume segment or, due to ergodicity, as the time average of a single molecule orientation at a given position. The orientations $\mathbf{n}(\mathbf{r}, t)$ and $-\mathbf{n}(\mathbf{r}, t)$ are equivalent. This is due to the fact that the molecules either have a center of inversion or, if they do not, they have equal probability of pointing parallel or anti-parallel to any given direction [7].

Because of thermal fluctuations, the molecules are not perfectly aligned to the director. Instead, there is a distribution of molecular orientations [5]. From this distribution, one can know the state of alignment of the molecules and extract a degree of order for the system.

In a reference frame where the z-axis is chosen to coincide with the direction of $\mathbf{n}$, the molecular orientations relative to the director are specified by the polar and azimuthal angles (θ, ϕ), as depicted in Fig. 2.1. The distribution function for the orientations is then $g(\theta, \phi)$. $g(\theta, \phi)d\Omega$ represents the probability of finding molecules

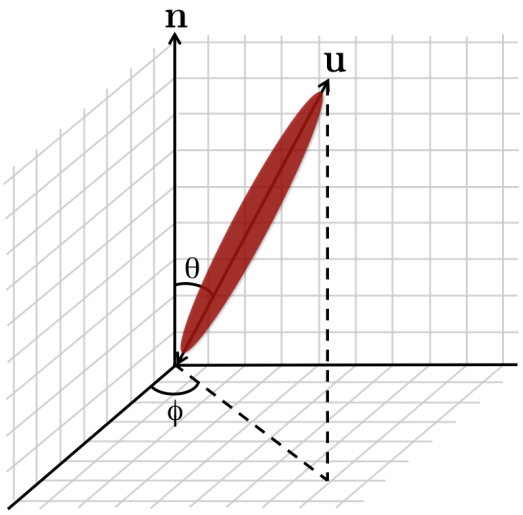

Figure 2.1: Polar and azimuthal angles, (θ, ϕ), that define the orientation $\mathbf{u}$ of the molecules, relative to the director $\mathbf{n}$.

in a infinitely small solid angle $d\Omega = \sin\theta d\theta d\phi$ around the direction (θ, ϕ) [5]. In this work, we shall only consider uniaxial phases, i.e. with a single preferred axis around which the system is rotationally invariant [7]. For uniaxial phases, there is complete cylindrical symmetry around $\mathbf{n}$ and, therefore, the distribution function is independent of the angle ϕ, $g(\theta, \phi) = g(\theta)$. Also, due to the symmetry $\mathbf{n} = -\mathbf{n}$, $g(\theta) = g(\pi - \theta)$. Thus, for this distribution function, the average of the scalar product between the molecular orientations $\mathbf{u}$ and $\mathbf{n}$ is [5].

$$\langle \mathbf{u} \cdot \mathbf{n} \rangle = \langle \cos\theta \rangle = \int g(\theta) \cos\theta d\Omega = 0 \ . \tag{2.1}$$

Here, $\langle . \rangle$ represents the ensemble average.

Given that the average projection of the molecular orientations $\mathbf{u}$ onto the director is equal to zero, this quantity does not provide any information about the state of alignment in the liquid crystal phase.

To characterize the order, one must resort to higher multipoles. The first multipole giving a non-zero result is the quadrupole

$$S = \frac{1}{2}\langle 3\cos^2\theta - 1 \rangle = \int g(\theta)\frac{1}{2}\left(3\cos^2\theta - 1\right) d\Omega \ . \tag{2.2}$$

S is called the scalar order parameter, with θ representing the angle of deviation from the director.

The values of S lie in the interval $\left[-\frac{1}{2}, 1\right]$. The value $S = 1$ represents a perfectly ordered state, $S = -\frac{1}{2}$ represents an arrangement where the molecules are aligned

perpendicular to the director (which happens for disk-like molecules), and the value $S = 0$ corresponds to a perfectly disordered, or isotropic, state. Ergo, S distinguishes between the isotropic and anisotropic phases.

The state of the system is completely specified by the knowledge of the director $\mathbf{n}$ and the scalar order parameter S. These two quantities complement each other, providing information about the direction of alignment of the molecules and the degree of order around that direction. S and $\mathbf{n}$ can be combined in a single order parameter. Because of the inversion symmetry between $\mathbf{n}$ and $-\mathbf{n}$, any order parameter must be an even function of $\mathbf{n}$. Therefore, a vector order parameter is insufficient. A more suitable order parameter can be introduced as a second-rank tensor. The tensorial order parameter is defined, for an uniaxial nematic, as

$$Q_{\alpha\beta} = \frac{S}{2}\left(3n_\alpha n_\beta - \delta_{\alpha\beta}\right), \tag{2.3}$$

where $\alpha, \beta = x, y, z$ and $\delta_{\alpha\beta}$ is the Kronecker delta.

By definition, and as a consequence of the properties of the director, the $\mathbf{Q}$ tensor is symmetric $Q_{\alpha\beta} = Q_{\beta\alpha}$ and traceless $Q_{\alpha\alpha} = 0$. [1] Also, in the isotropic phase the order parameter is zero as expected, $Q_{\alpha\beta,iso} = 0$. The scalar order parameter S is the largest eigenvalue of $\mathbf{Q}$, with corresponding eigenvector $\mathbf{n}$. The other two eigenvalues are equal to $-\frac{S}{2}$ and have corresponding eigenvectors perpendicular to $\mathbf{n}$. Note that if biaxiality is considered, the definition of the order parameter is $Q_{\alpha\beta} = \frac{S}{2}\left(3n_\alpha n_\beta - \delta_{\alpha\beta}\right) + \frac{B}{2}\left(l_\alpha l_\beta - m_\alpha m_\beta\right)$ [35], where $\mathbf{n}$, $\mathbf{l}$, and $\mathbf{m}$ form a local orthonormal triad. The direction of maximum orientational order is still associated with $\mathbf{n}$, but the cylindrical symmetry around $\mathbf{n}$ is broken. Even if the molecules have cylindrical symmetry, biaxiality may arise from spatial non-uniformities on the plane perpendicular to $\mathbf{n}$ and results in a parameter $B \neq 0$. For non-zero biaxiality, the $\mathbf{Q}$ tensor has three different eigenvalues: S, $-\frac{1}{2}S + B$, and $-\frac{1}{2}S - B$.

Because it does not deal with the director $\mathbf{n}$ and the scalar order parameter S independently, the tensorial approach with order parameter $\mathbf{Q}$ is appropriate for the description of samples with spatially varying degree of order $S = S(\mathbf{r})$. Therefore, the tensorial approach is needed in many problems involving the interaction with surfaces, and when topological defects are present.

[1] The number of components of a general 3×3 second-rank tensor is 9. The $\mathbf{Q}$ tensor however, being symmetric and traceless, has only five independent components. Thus, the $\mathbf{Q}$ tensor is often explicitly represented as $\mathbf{Q} = \begin{bmatrix} q_1 & q_2 & q_3 \\ q_2 & q_4 & q_5 \\ q_3 & q_5 & -(q_1+q_4) \end{bmatrix}$, with q_1, q_2, q_3, q_4 and q_5 being the only independent components. This form is useful in the calculations as it reduces the number of variables to solve for.

2.2 Landau-de Gennes Model

Once the appropriate order parameter of the system is defined (here the $\mathbf{Q}$ tensor), one can construct a free energy functional $\mathcal{F}$ for nematic and cholesteric liquid crystals. The free energy functional is an integral over the volume of the sample of a free energy density f, expressed as a function of $\mathbf{Q}$. The free energy density is made of two contributions: f_{ord}, a Landau free energy that models the transition between the isotropic phase and the ordered liquid crystal phase, and f_{elas}, an elastic contribution that penalizes distortions from the preferred alignment

$$\mathcal{F} = \int \left[f_{ord} + f_{elas} \right] dV \ . \tag{2.4}$$

2.2.1 The nematic-isotropic transition

In the spirit of Landau theories, one can assume that the free energy density $f_{ord}(P, T, \mathbf{Q})$ is an analytic function of the order parameter tensor $\mathbf{Q}$. Here, P represents the pressure and T the temperature. For thermotropic liquid crystals, the temperature is the main parameter driving the transition between different mesophases. Near the transition temperature, and to the extent that $\mathbf{Q}$ is a small parameter, the free energy density $f_{ord}(P, T, Q_{\alpha\beta})$ may be expanded in a power series of the order parameter.

The ordered phase is invariant under uniform rotations of the group O_2 on the plane perpendicular to the director. Rotations outside of this plane alter the director. However, because the direction of alignment is arbitrary in space, the state generated by such rotation corresponds to an equivalent system, which should have the same free energy. This symmetry imposes that $f_{ord}(P, T, Q_{\alpha\beta})$ must be invariant under the group $SO(3)$ of all rotations [7]. Since $Q_{\alpha\beta}$ transforms like a tensor under the rotation group, the terms of the expansion allowed by symmetry must be scalar functions of $Q_{\alpha\beta}$. The minimal free energy volume density f_{ord} needed to model the nematic-isotropic transition reads

$$f_{ord} = f_{iso} + \frac{1}{2} A \ Q_{\alpha\beta} Q_{\beta\alpha} + \frac{1}{3} B \ Q_{\alpha\beta} Q_{\beta\gamma} Q_{\gamma\alpha} + \frac{1}{4} C \ \left(Q_{\alpha\beta} Q_{\beta\alpha} \right)^2 \ , \tag{2.5}$$

which is correct to fourth order in $Q_{\alpha\beta}$. Summation over repeated indices is assumed. f_{iso} is the free energy density of the isotropic phase. The first order term in this expansion would simply be the trace $Q_{\alpha\alpha}$ which is, by definition, equal to zero. Thus, there is no linear term in the free energy. As a consequence of this symmetry, the state of minimum energy has a state of zero $Q_{\alpha\beta}$, that is to say, isotropic. There

is just one distinct invariant of the second, third, and fourth orders. Other forms (such as $Q_{\alpha\beta}Q_{\beta\gamma}Q_{\gamma\delta}Q_{\delta\alpha}$) are strictly proportional to the ones included in (2.5) for a 3×3 symmetric and traceless tensor [7].

Assuming an uniaxial nematic, the trace invariants of the order parameter tensor simplify to $Q_{\alpha\beta}Q_{\beta\alpha} = \frac{3S^2}{2}$, and $Q_{\alpha\beta}Q_{\beta\gamma}Q_{\gamma\alpha} = \frac{3S^3}{4}$. Thus f_{ord} can be rewritten as a function of the scalar order parameter S:

$$f_{ord} = \frac{3}{4}A\ S^2 + \frac{1}{4}B\ S^3 + \frac{9}{16}C\ S^4\ . \tag{2.6}$$

The energy f_{iso} of the isotropic phase has been taken as the zero of the energy scale. The coefficients A, B, and C are nematic material properties and are, in general, functions of the pressure P and temperature T. In the nematic phase, both A and B are negative and only $C > 0$ ensures that the free energy density functional is bounded from below.

Typical to Landau-type theories, this model equation of state predicts a phase transition near the temperature where A vanishes. It is normally assumed that A has the form $A = a(T - T^*)$, where T^* is the supercooling temperature [7]. The coefficients B and C need have no particular properties near T^*, and will be regarded as constants. Under this assumption, A is the only pre-factor having a temperature dependence and, therefore, drives the nematic-isotropic transition. Typical values for 5CB, a nematic commonly used in experimental studies, are $A = -0.1694MJ/m^3$, $B = 0.816MJ/m^3$, $C = 0.45MJ/m^3$.

The nematic-isotropic transition is of first order [7]. This is related with the meaning of the sign of the scalar order parameter S. States with $S > 0$ correspond to rod-like configuration where the molecules have their long axis aligned with the director, while states with $S < 0$ correspond to a disk-like configuration where the molecules are aligned perpendicular to the director. The two situations are depicted in Fig. 2.2. The states with $S > 0$ and $S < 0$ are not related by any symmetry operation. Thus, there is no reason for them to have the same energy. The lack of symmetry between states with positive and negative scalar order parameter is the basis of the first order transition [7] and it is modelled in the free energy by the third order term S^3. The role of this term is exactly to break the symmetry between states with $S > 0$ and $S < 0$.

The interpretation of the Landau expansion terms in expression (2.6) for the free energy density f_{ord} is now clear: first term drives the transition, second term ensures asymmetry by breaking the $S > 0$ to $S < 0$ invariance, and the third term bounds the values of f_{ord} from below.

The minimization of the free energy corresponding to the density (2.6) gives the

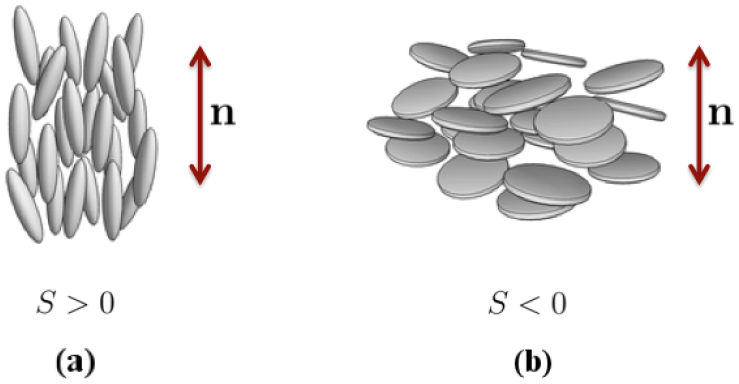

Figure 2.2: (a) Nematic alignment for rod-like molecules. Molecular long axis are aligned parallel to the director, corresponding to a positive value of the scalar order parameter $S > 0$. (b) Nematic alignment for disk-like molecules. The director is perpendicular to the molecules, corresponding to a negative value of the scalar order parameter $S < 0$.

equilibrium scalar order parameter S_{eq} in terms of the material parameters

$$S_{eq}(A,B,C) = \begin{cases} 0, & T > T_{NI} \\ \frac{1}{2}\left[-\frac{B}{3C} + \sqrt{\left(\frac{B}{3C}\right)^2 - \frac{8A}{3C}}\right], & T < T_{NI}, \end{cases} \tag{2.7}$$

where T_{NI} is the nematic-isotropic transition temperature.

It is useful to rescale the energy by defining the quantities [36]

$$\tilde{Q}_{ij} = \frac{6C}{B} Q_{ij}, \tag{2.8}$$

$$\tilde{f}_{ord} = \frac{24^2 c^3}{B^4} f_{ord}. \tag{2.9}$$

Also, a dimensionless temperature τ can be introduced so that the nematic phase is stable for $\tau < 1$

$$\tau = \frac{24AC}{B^2}. \tag{2.10}$$

With the previous definitions, the rescaled free energy as a function of the rescaled scalar order parameter is given by

$$\tilde{f}_{ord} = \tau \tilde{S}^2 - 2\tilde{S}^3 + \tilde{S}^4, \tag{2.11}$$

and the equilibrium scalar order parameter for the nematic phase becomes

$$\tilde{S}_{eq} = \frac{3}{4}\left(1 + \sqrt{1 - \frac{8}{9}\tau}\right). \tag{2.12}$$

The minus sign, explicitly expressed in Eq. (2.11), comes from the breaking of the invariance between $\tilde{S} > 0$ and $\tilde{S} < 0$.

The characteristics of the $\tilde{f}_{ord}$ free energy density for the different temperature regimes, including the metastability limits, are presented in Fig. 2.3. The isotropic-nematic transition occurs at the critical temperature τ_c, for which the ordered $\tilde{S} = 0$ and disordered $\tilde{S} \neq 0$ states are equally probable. Above the transition temperature, and below the superheating temperature τ^{**}, the nematic phase is metastable and the isotropic phase is stable, corresponding to the lowest value of the free energy. Above the superheating temperature τ^{**}, the free energy has one only minimum for $\tilde{S} = 0$. Below the transition temperature τ_c, and above the supercooling temperature τ^*, the free energy has two minima: the isotropic state, which is metastable, and the ordered state, which is stable. Below the supercooling temperature τ^*, the only minimum of the free energy corresponds to the nematic phase. The transition is of first order, as can be seen by the energy barrier between the two states that minimize the free energy.

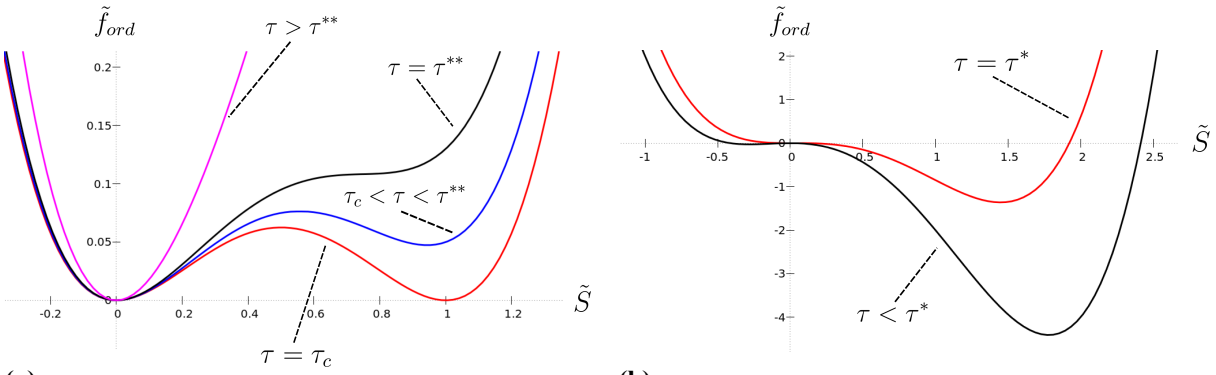

Figure 2.3: Free energy density $\tilde{f}_{ord}$ as a function of the scalar order parameter $\tilde{S}$ for different temperatures τ, for the isotropic-nematic transition. The transition is first order. Note the limits of metastability for supercooling (τ^*) and superheating (τ^{**}). (a) High temperature regime. For τ above the superheating temperature τ^{**} only the isotropic phase ($\tilde{S} = 0$) is stable. When the temperature decreases to τ^{**}, the nematic phase becomes metastable. On the transition temperature τ_c, the isotropic and nematic phases are equiprobable. The nematic phase is stable below τ_c. (b) Low temperature regime. The isotropic phase is no longer metastable below the supercooling temperature τ^*.

2.2.2 Elastic energy

Because the molecules tend to align along an average direction, the lowest energy state for the nematic phase is homogeneously oriented throughout the sample. Any deformations of this uniform director field are penalised with an increase of the free energy. Therefore, nematics act as effective elastic materials when their orientational ordering is subjected to spatial variations. If the deviation in the molecular orientations varies slowly in space on the molecular distance scale, one is able to describe the distortion of the liquid crystal with a continuum elastic theory. Here the deformations are not the changes of the position of neighbouring points as in solids, but are the changes in the orientation between two neighbouring points.

Three basic types of deformations can be identified: splay, twist and bend. Each one corresponds to a non-vanishing term in the derivatives of the director $\mathbf{n}$. The representation of the three basic deformations is shown in Fig. 2.4.

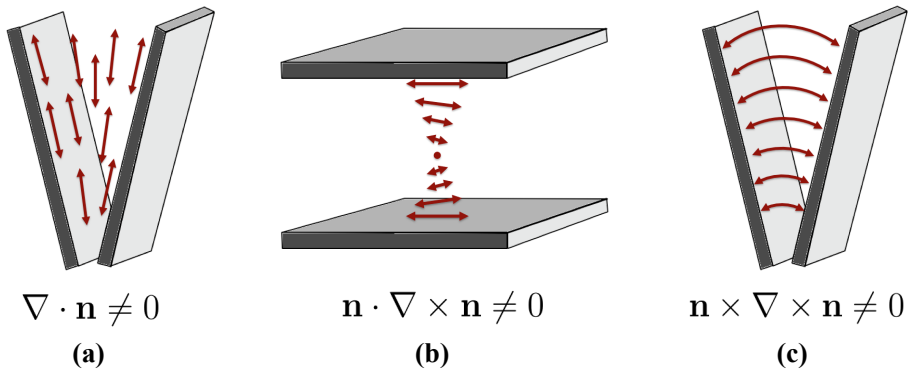

Figure 2.4: Elastic deformation modes: (a) splay, (b) twist, and (c) bend.

The free energy that models these deformations can be constructed by expanding around the uniform state in derivatives of the director field. Given that the characteristic dimensions of the deformations are large compared to molecular dimensions, the spatial derivatives of the director $\partial_\alpha n_\beta$ are small quantities. It usually suffices that only first and second order terms in the expansion of the free energy density are retained. Thus, the free energy density can be written generally as [37]

$$f_{elas} = K_{\alpha\beta}\ \partial_\alpha n_\beta + K_{\alpha\beta\gamma\delta}\ (\partial_\alpha n_\beta)\,(\partial_\gamma n_\delta) + K_{\alpha\beta\gamma}\ \partial_\alpha \partial_\beta n_\gamma, \tag{2.13}$$

where the indices $\alpha, \beta, \gamma, \delta$ represent the cartesian coordinates.

Again, the free energy must be invariant under the symmetry operations that leave the nematic phase unchanged. Thus, for a nematic, the energy density f_{elas} is invariant under uniform rotations of the whole sample and under the inversion

operations $\mathbf{n} \to -\mathbf{n}$ and $\mathbf{x} \to -\mathbf{x}$. The tensors $K_{\alpha\beta}$, $K_{\alpha\beta\gamma}$, and $K_{\alpha\beta\gamma\delta}$ must be composed of all possible invariants constructed with the director n_α, the Kronecker delta function $\delta_{\alpha\beta}$ and Levi-Civita tensor $\varepsilon_{\alpha\beta\gamma}$, that are allowed by symmetry. Analysing all the possibilities for the $K_{\alpha\beta}$, $K_{\alpha\beta\gamma}$, and $K_{\alpha\beta\gamma\delta}$ tensors that are compatible with the symmetries of the free energy, and excluding those that can be integrated as surface terms, one can identify the following independent terms

$$\begin{aligned} (\partial_\alpha n_\alpha)(\partial_\beta n_\beta) &= (\nabla \cdot \mathbf{n})^2, & (2.14)\\ (\partial_\alpha n_\beta)(\partial_\beta n_\alpha) &= (\nabla \cdot \mathbf{n})^2 + (\mathbf{n} \cdot \nabla \times \mathbf{n})^2 + (\mathbf{n} \times \nabla \times \mathbf{n})^2, & (2.15)\\ n_\alpha n_\beta (\partial_\alpha n_\gamma)(\partial_\beta n_\gamma) &= (\mathbf{n} \times \nabla \times \mathbf{n})^2. & (2.16) \end{aligned}$$

These invariants can be grouped to construct the Frank-Oseen free energy density, where the basic deformations (Fig. 2.4) are easily identified.

$$\left[f^{FO}_{elas}\right]_{nem} = \frac{1}{2}K_1 (\nabla \cdot \mathbf{n})^2 + \frac{1}{2}K_2 (\mathbf{n} \cdot \nabla \times \mathbf{n})^2 + \frac{1}{2}K_3 (\mathbf{n} \times \nabla \times \mathbf{n})^2. \quad (2.17)$$

K_1, K_2, and K_3 are the elastic constants for splay, twist, and bend deformations, respectively.

Cholesteric liquid crystals are made of chiral molecules and therefore for this type of liquid crystal there is no mirror symmetry $\mathbf{x} \to -\mathbf{x}$. This means that there is one more term allowed by the symmetry

$$\varepsilon_{\alpha\beta\gamma} n_\gamma \partial_\alpha n_\beta = \mathbf{n} \cdot (\nabla \times \mathbf{n}). \quad (2.18)$$

Introducing the term (2.18) in the elastic free energy, one finds the elastic free energy density for the colesteric

$$\left[f^{FO}_{elas}\right]_{chol} = \frac{1}{2}K_1 (\nabla \cdot \mathbf{n})^2 + \frac{1}{2}K_2 (\mathbf{n} \cdot \nabla \times \mathbf{n} - q_0)^2 + \frac{1}{2}K_3 (\mathbf{n} \times \nabla \times \mathbf{n})^2, \quad (2.19)$$

$q_0 = \frac{2\pi}{P_0}$, with P_0 the cholesteric pitch, this is, the length at witch the director turns by 2π. q_0 vanishes for a nematic.

The Frank-Oseen free energy can be extended to include the mixed terms f_{13} [38] and f_{24} [39], which are also allowed by symmetry.

$$\begin{aligned} f_{13} &= K_{13} \nabla \cdot [\mathbf{n}(\nabla \cdot \mathbf{n})] & (2.20)\\ f_{24} &= -K_{24} \nabla \cdot [\mathbf{n}(\nabla \cdot \mathbf{n}) + \mathbf{n} \times (\nabla \times \mathbf{n})] & (2.21) \end{aligned}$$

The elastic constants K_{13} and K_{24} refer to splay-bend and saddle-splay distortions,

respectively. The f_{13} and f_{24} terms are designated divergence volume density terms because they can be transformed into surface terms by the direct application of the Gauss theorem. For that reason, it is considered that their effect on the bulk behaviour of the liquid crystal can be treated with a renormalization of the surface anchoring. We will not consider the contribution of the mixed terms in the development of our model.

The vectorial approach to the construction of the elastic free energy density allows a direct characterization of the three elastic distortion modes. However, when describing samples where not only the director $\mathbf{n}$ varies in space but also the scalar order parameter S depends on the position, the tensorial order parameter $Q_{\alpha\beta}$ is needed. In the tensorial approach, the spacial derivatives are also assumed to be small and the free energy density is expanded into series over invariant terms of $Q_{\alpha\beta}$ and $\partial_\alpha Q_{\alpha\beta}$. The procedure to construct the free energy density is the same as for the vectorial approach, one needs to find quantities that are invariants under the same symmetry operations to as the free energy.

The simplest elastic free energy that models all the same distortions as the Frank-Oseen free energy is:

$$f_{elas} = \frac{1}{2}L_1\partial_\gamma Q_{\alpha\beta}\partial_\gamma Q_{\alpha\beta} + \frac{1}{2}L_2\partial_\beta Q_{\alpha\beta}\partial_\gamma Q_{\alpha\gamma} + \frac{1}{2}L_3 Q_{\alpha\beta}\partial_\alpha Q_{\gamma\delta}\partial_\beta Q_{\gamma\delta} + 2L_1 q_0 \varepsilon_{\alpha\delta\gamma} Q_{\alpha\beta}\partial_\beta Q_{\gamma\beta} \tag{2.22}$$

where L_1, L_2 and L_3 are tensorial elastic constants, x_α are Cartesian coordinates, and summation over repeated indices is assumed. Three elastic constants are introduced in order to account for the three basic deformation modes. Again, the term proportional to q_0 is only present for the cholesteric phase and it vanishes in the nematic. The L_i are independent of the degree of order S and should be interpreted as the direct strength of the inter-molecular interactions.

The relation between elastic constants in the vectorial and tensorial frameworks is obtained when $Q_{\alpha\beta}$ in the free energy density (2.22) is replaced by the uniaxial nematic definition $Q_{\alpha\beta} = \frac{S}{2}(3n_\alpha n_\beta - \delta_{\alpha\beta})$. By making use of the identities $n_\alpha n_\alpha = 1$ and $n_\alpha \frac{\partial n_\alpha}{x_\gamma} = 0$, the Frank-Oseen free energy, in terms of the director $\mathbf{n}$, is recovered, given the correspondences [40]

$$\begin{aligned} L_1 &= \frac{K_3 + 2K_2 - K_1}{9S^2}\,, \\ L_2 &= \frac{4(K_1 - K_2)}{9S^2}\,, \\ L_3 &= \frac{2(K_3 - K_1)}{9S^2}\,. \end{aligned} \tag{2.23}$$

Elastic free energy volume densities are complex spatially dependent functionals when used with all three elastic constants. A common approximation to simplify the free energy density functional is to use the one elastic constant approximation which sets $K_1 = K_2 = K_3$ and, consequently, $L_1 = L$, $L_2 = L_3 = 0$. Typical values for the elastic constants in 5CB are $L_1 = 6 \times 10^{-12} J/m$ and $L_2 = 0 J/m$. (We assume the nematic 5CB material parameters in order construct a simple cholesteric model in which we allow a spontaneous twist.) Within the one constant approximation, the restoring forces that oppose the three basic deformations have equal strength. The free energy f_{elas} is then written as:

$$f_{elas} = \frac{1}{2} L \partial_\gamma Q_{\alpha\beta} \partial_\gamma Q_{\alpha\beta} + 2 L q_0 \varepsilon_{\alpha\delta\gamma} Q\alpha\beta \partial_\beta Q_{\gamma\beta} \tag{2.24}$$

The ratio of the two energy contributions in the Landau-de Gennes free energy introduces a spatial scale for the variation of the nematic degree of order. This characteristic length scale is referred to as the nematic correlation length ξ. Typically, ξ is of the order of a few nanometres, and it is related to the material parameters by the expression [36]

$$\xi^2 = \frac{L_1 8C}{B^2}. \tag{2.25}$$

The correlation length plays a very important role in the discussion of topological defects as it roughly determines their size.

Rescaling all the positions by $\tilde{\mathbf{r}} = \frac{\mathbf{r}}{\xi}$, and the tensorial order parameter and free energy density according to (2.9), the elastic free energy takes the form

$$\tilde{f}_{elas} = \frac{1}{3 + 2\kappa} \left(\tilde{\partial}_\gamma \tilde{Q}_{\alpha\beta} \tilde{\partial}_\gamma \tilde{Q}_{\alpha\beta} + \kappa \tilde{\partial}_\beta \tilde{Q}_{\alpha\beta} \tilde{\partial}_\gamma \tilde{Q}_{\alpha\gamma} \right), \tag{2.26}$$

where $\kappa = \frac{L_2}{L_1}$. The one elastic constant approximation corresponds to setting $\kappa = 0$.

2.3 Surface anchoring

Interfaces with solid, liquid or gas materials affect liquid crystal ordering by imposing a preferred degree of order and a preferred molecular orientation. Such behaviour is usually referred to as anchoring. Three typical situations are: *i)* homeotropic anchoring, where the preferred, or "easy", on average orientation corresponds to $\mathbf{n}$ normal to the interface, *ii)* planar anchoring, where the preferred average orientation corresponds to $\mathbf{n}$ lying in one particular direction parallel to the interface, and *iii)* planar degenerate anchoring, where all the planar orientations for $\mathbf{n}$ are equivalent

easy directions.

Uniform, or non-degenerate, surface anchoring is modelled by using a Nobili-Durand [41] like surface free energy density functional f_{surf}:

$$f_{surf} = \frac{1}{2} W \left(Q_{\alpha\beta} - Q^0_{\alpha\beta} \right)^2 , \tag{2.27}$$

where W is the uniform surface anchoring strength and $Q^0_{\alpha\beta}$ is the surface preferred order parameter tensor. f_{surf} penalizes all deviations of $Q_{\alpha\beta}$ from $Q^0_{\alpha\beta}$. Therefore $Q^0_{\alpha\beta}$ imposes not only the preferred direction at the surface, the easy axis, but also the surface degree of order. Because f_{surf} is proportional to the sum of the squares of the components of $Q - Q^0$, it has, for $W > 0$, a unique minimum for $Q = Q^0$.

Planar degenerate anchoring describes the tendency of a substrate to favour the common alignment of the molecules along any direction parallel to its surface. To model such situation, it is necessary to include terms of order higher than two. Going up to fourth order ensures that the surface free energy is bounded from below. This is also the lowest order for the bulk free energy to describe correctly the nematic-isotropic transition. Such degenerate surface functional was introduced by Fournier and Galatola [42]

$$f^{deg}_{surf} = W_1 \left(\tilde{Q}_{\alpha\beta} - \tilde{Q}^{\perp}_{\alpha\beta} \right)^2 + W_2 \left(\tilde{Q}_{\alpha\beta} \tilde{Q}_{\beta\alpha} - \frac{3}{2} S^2_{surf} \right)^2 , \tag{2.28}$$

where W_1 and W_2 are two surface anchoring constants, S_{surf} is the surface-preferred degree of order, $\tilde{Q}_{\alpha\beta} = Q_{\alpha\beta} + \frac{S_{surf}}{2}\delta_{\alpha\beta}$, and $\tilde{Q}^{\perp}_{\alpha\beta} = P_{\alpha\gamma}\tilde{Q}_{\gamma\delta}P_{\delta\beta}$, with $P_{\alpha\beta} = \delta_{\alpha\beta} - \nu_\alpha\nu_\beta$ and ν_α the surface normal. Typical values for the anchoring constants are $W_i = 0.01 J/m^2$. The first term imposes that $\tilde{Q}_{\alpha\beta}$ coincides with its projection on the substrate $\tilde{Q}^{\perp}_{\alpha\beta}$. The second term addresses the degree of order and imposes that the trace of the square of $\tilde{Q}_{\alpha\beta}$ coincides with S^2_{Surf}. These two conditions are necessary and sufficient to obtain the condition of planar degenerate anchoring.

The rescaling relations used in the previous sections simply rescale the anchoring constants by $\tilde{W}_i = \frac{16 W_i C}{B^2 \xi}$.

The free energy that describes the order f_{ord}, the elastic free energy f_{elas}, and the anchoring free energy f_{surf} are combined into a single functional $\mathcal{F}$, as defined in Eq. (2.4). The Landau-de Gennes model is the central phenomenological model for nematic and cholesteric liquid crystals at micron and sub-micron mesoscale as it incorporates both elasticity and spatial variation of the nematic degree of order. The equilibrium configuration of the nematic or cholesteric in an arbitrary geometry is obtained by the minimization of this free energy in the volume of the sample. This is

the approach followed in the present work. We use numerical methods to discretize the sample space and minimize the free energy, obtaining the stable (or, at least, metastable) configurations of the confined cholesteric.

2.4 Topological Defects

The Landau-de Gennes free energy models the orientational ordering of the molecules in the nematic phase. As a result of this ordering, the minimum energy configuration for a nematic in bulk is uniformly aligned. The preferred direction of ordering is, however, arbitrary and it is only fixed in practice by an external field or by interaction with a surface. Distortions from the homogeneously aligned state are penalised by an increase of the free energy. Although configurations with distortions have a higher free energy, they are the lowest energy state in situations where the alignment with boundary conditions and external fields has to be obeyed.

When the liquid crystal is confined, there may not be a configuration that satisfies the boundary conditions, while including only continuous distortions. In such cases there is the nucleation of topological defects, i.e., singularities in the orientational field.

Topological defects appear in physics as a consequence of broken continuous symmetry and they have different names depending on the symmetry that is broken and the particular system in question. Defects in the orientatonal order, such as in nematic or cholesteric liquid crystals, are called disclinations [7]. The defects are topological when they cannot be removed by a continuous deformation of the order parameter. This is different from what happens with the elastic distortions. A configuration that exhibits elastic distortions without singularities can be returned to the aligned state by a sequence of distortions in which the director at each point changes by an infinitesimal amount relative to the previous configuration. An attempt to align the molecules in a configuration including topological defects would imply a discontinuous change of the orientations at some point.

A topological defect is characterized by a small core region where the order is destroyed and a far field region where the orientation varies slowly in space. This singularity could be removed by cutting a hole of radius ξ_0 out of the material, around the core region. An alternative approach is to have the magnitude of the scalar order parameter go to zero at the core and rise to its equilibrium value at a radius ξ_0. Since the order parameter is zero at the origin, the director is no longer defined there, and the mathematical singularity has been removed. This is an argument for the use of the tensorial order parameter in situations that involve

topological defects. At the core, the director is not defined but the tensor $Q_{\alpha\beta}$ has the value $Q_{\alpha\beta} = 0$ because $S = 0$. In this sense, the core of the defect is like a small region of isotropic phase and has dimensions of the correlation length ξ, since this is the scale of variation of the degree of order.

Topological defects have the property that its presence can be determined by measurements of an appropriate field on any surface enclosing its core. For nematics and cholesterics, this is the director field. In 2D, the number of times that the director completes a rotation by an angle of 2π measured on any closed circuit around the defect core is the topological charge m. Because the circuit must be a closed loop, the topological charge may only take on a discrete set of values. In nematics and cholesterics, due to the equivalence between positive and negative directions of the director, the topological charge may assume half integer numbers. The sign of this charge is positive if the director rotates in the direction of circulation of the path and negative otherwise.

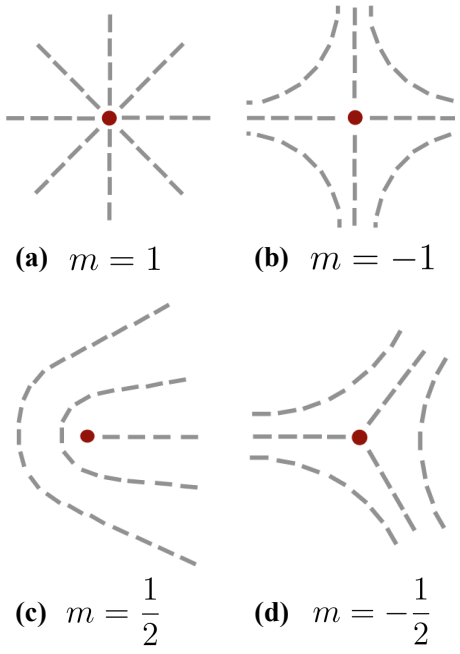

Figure 2.5: Schematics of the director field in configurations with topological defects with charges $m = 1$ (a), $m = -1$ (b), $m = \frac{1}{2}$ (c), and $m = -\frac{1}{2}$ (d). The grey rods represent the director orientation and the red dots represent the cores of the defects.

Defects appear in the equilibrium configuration of nematics and cholesterics because they cannot be removed without making discontinuous changes in the configuration. They are topologically stable. However, their presence increases the free energy. This increase in the free energy is divided into two contributions, one from the decrease of order at the core of the defect, and the second from the far field

elastic distortions. For a defect in the plane, the total free energy is, in the one elastic approximation $K_1 = K_2 = K_3 = K$[7]

$$\begin{aligned} E &= E_{core} + E_{elastic} \\ &= \frac{\pi K m^2}{2} + \pi K m^2 \ln\left(\frac{R}{\xi_0}\right), \end{aligned} \tag{2.29}$$

where R is the dimension of the sample and ξ_0 the dimension of the core of the defect.

In cholesteric liquid crystals, the director twists periodically on a direction perpendicular to itself. Because of this escape to the third dimension, disclinations in cholesterics can be singular or non-singular [34]. We shall distinguish three classes: λ^m, τ^m, and χ^m (see Fig. 2.6). In the λ and τ disclinations there is no twist of the director along the disclination. λ disclinations are non-singular and τ disclinations are singular. The director twists along the χ disclination, resulting in planes with and without singularities.

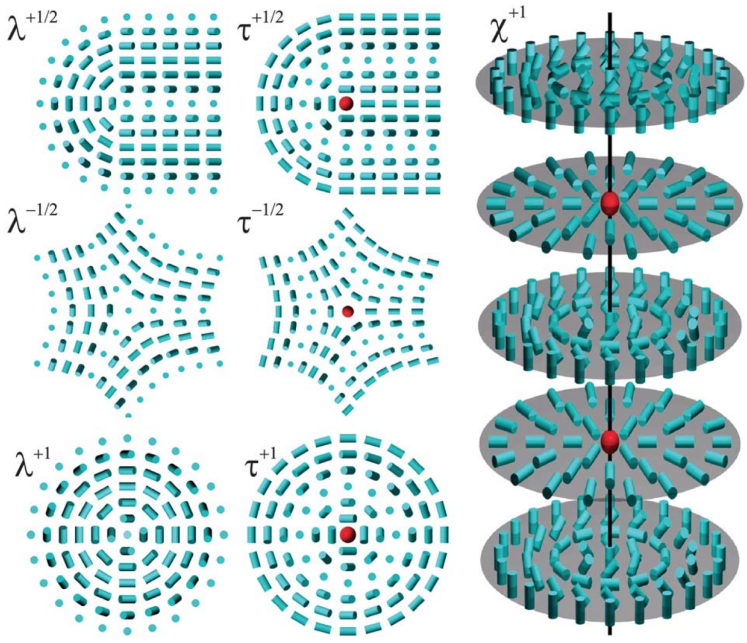

Figure 2.6: Schematic representation of cholesteric disclination lines λ^m, τ^m, and χ^m with various topological charges m. The director is shown with blue cylinders and the red spheres represent regions with lower order parameters. The core of the χ disclination is drawn as a black line. Figure obtained from Fig.1 of [34].

Curved geometries introduce new constraints to the system, since the packing is not the same as in a flat geometry. Let us consider, for illustration, the canonical example of the packing of hexagons. On a plane, it is possible to arrange hexagonal

cells in a honeycomb pattern, filling the space with no frustrations as in Fig. 2.7(a). However, on the surface of a sphere, it is not possible to do the same. A known example of a pattern that can fill such curved space is the soccer ball with 12 pentagon panels dispersed among hexagons, as shown in Fig. 2.7(b).

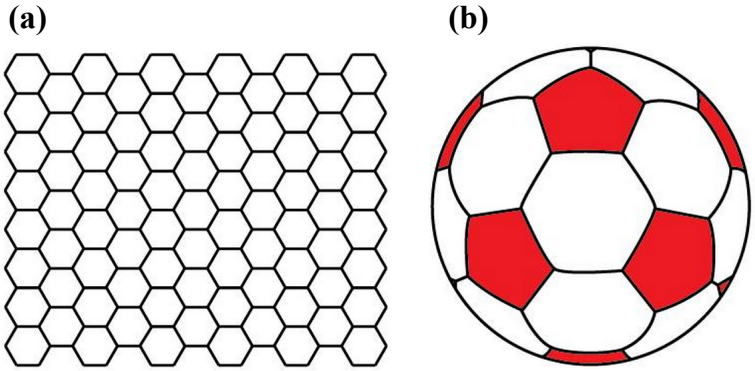

Figure 2.7: Packing of hexagonal cells in a flat space (a) and on the surface of a sphere (b). Figure obtained from Fig.1 of [27].

The flat space and the surface of a sphere have different topologies. The topological shape of a space is described by a topological invariant called the Euler characteristic χ (or Euler-Poincaré characteristic). The Euler characteristic can be given, for closed surfaces, by the expression [43]

$$\chi = 2\,(1 - g)\,, \tag{2.30}$$

where g is the genus or number of handles of the surface. For instance, the sphere has genus $g = 0$ and Euler characteristic $\chi = 2$. The torus has genus $g = 1$ and Euler characteristic $\chi = 0$.

Analogously to the packing of geometrical shapes like the hexagons, we can align rods that represent the director field. When we align rods on a curved surface there is a topological constraint that fixes the net charge of topological defects that must be present on the surface. This is expressed in the Poincaré - Hopf Theorem [43] stating that the sum of the topological charges must be equal to the Euler characteristic of the surface

$$\sum_i m_i = \chi = 2\,(1 - g)\,, \tag{2.31}$$

where m_i is the topological charge of each defect.

In particular, it is impossible to align rods smoothly on a sphere without having any sources or sinks (see Fig. 2.8). Aligned configurations on the surface of a sphere

must have topological defects where it is impossible to define the orientation of the field. Figure 2.8 shows two types of bipolar configurations on a sphere. Two defects are located at opposite poles and the director is aligned along the meridians (Fig. 2.8 (b)) or parallels to the equator (Fig. 2.8 (c)).

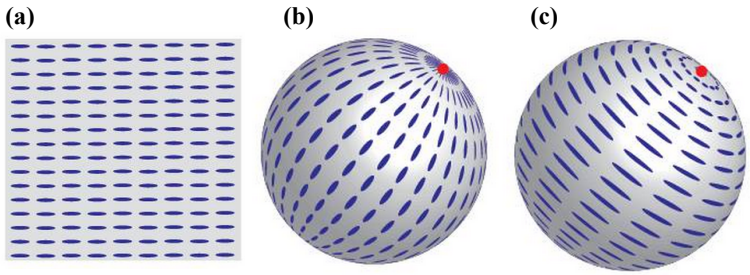

Figure 2.8: Example of rods arranged in parallel on flat (a), and on spherical surfaces (b) and (c). Figure obtained from Fig.3 of [27].

Unlike what happens on the surface of the sphere, on a torus the configurations of the director field must have zero net topological charge. This includes configurations with no defects like the two shown in Fig. 2.9. For planar alignment at the surface, the director can align with the torus (Fig. 2.9 (a)) or twist (Fig. 2.9 (b)) along it, all without having any region of reduced order. This is due to the fact that the torus has an Euler characteristic $\chi = 0$.

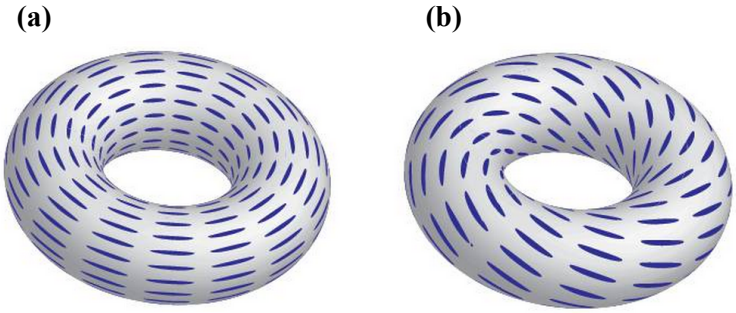

Figure 2.9: Schematic of rods packing on toroidal surface in axial (a) and twisted (b) configuration. Figure obtained from Fig.5 of [27].

Chapter 3

Numerical Methods

The main purpose of this thesis is to understand the behaviour of a cholesteric liquid crystal confined by curved surfaces. In order to do so, we analyse the equilibrium configurations of the cholesteric inside different curved domains.

Two main classes of systems are considered: systems with imposed cylindrical symmetry around an axis, and systems without cylindrical symmetry. For the first case, only a two-dimensional cross-section of the system is simulated. Because of the cylindrical symmetry, all other cross-sections can be obtained by a simple rotation transformation. For the systems without cylindrical symmetry, the fully three-dimensional domain must be considered.

The equilibrium configurations are obtained by the numerical minimization of the Landau-de Gennes free energy.

However, the minimization method is different for the systems simulated in two and three dimensions. In two dimensions we have used the commercial software COMSOL Multiphysics 3.5a [44] to solve numerically the Euler-Lagrange equations, which describe the stationary points of the Landau-de Gennes free energy, with a time relaxation scheme (Model A [7]). In three dimensions, we have used an in house code which implements the Finite Element Method with Adaptive Meshing to minimize the same Landau-de Gennes free energy with a limited-memory quasi-Newton technique [45].

The three-dimensional Finite Element Method allows us to obtain more precise and realistic results, and the Adaptive Meshing technique provides a high computational efficiency for the desired precision. However, with the two-dimensional models it is possible to isolate the effect of curvature in our analysis. Also, although not as powerful as the Finite Element Method, the COMSOL Multiphysics 3.5a allows us to alter the shape of the simulated domains very easily, facilitating the comparison between different cross-section confinements.

The details for the two kinds of methods are presented in this chapter, in Sections 3.1 and 3.2. In Section 3.3, we briefly outline the technique used to visualise the configurations.

3.1 Systems with cylindrical symmetry

The first step in setting up the system with imposed cylindrical symmetry is to deduce the equations that describe it. The time evolution equation for the tensor order parameter is given by

$$\frac{\partial}{\partial t}Q_{\alpha\beta} = \Gamma H_{\alpha\beta}, \tag{3.1}$$

where $Q_{\alpha\beta}$ are the components of the order parameter tensor $\mathbf{Q}$, $H_{\alpha\beta} = \frac{\delta\mathcal{F}}{\delta Q_{\alpha\beta}}$ is the molecular field tensor, and Γ is the relaxation constant. The condition for the relaxed system is, therefore, $H_{\alpha\beta} = 0$, which is equivalent to the Euler-Lagrange equations

$$\partial_i \left[\frac{\partial f}{Q_{\alpha\beta,i}}\right] - \frac{\partial f}{\partial Q_{\alpha\beta}} = 0, \tag{3.2}$$

where f is the reduced bulk free energy density (the tilde has been dropped to simplify the notation), $\partial_i = \frac{\partial}{\partial x_i}$, with $x_i = x, y, z$, and $Q_{\alpha\beta,i} = \partial_i Q_{\alpha\beta}$. Summation over repeated indices is assumed. Because we fix the boundary conditions in this case, we shall not consider the surface equations. Also, the free energy density contains only the order and elastic terms

$$\mathcal{F} = \int dV \left[f_{ord} + f_{elas}\right], \tag{3.3}$$

$$f_{ord} = \frac{2}{3}\tau Q_{\alpha\beta}Q_{\beta\alpha} - \frac{8}{3}Q_{\alpha\beta}Q_{\beta\gamma}Q_{\gamma\alpha} + \frac{4}{9}\left(Q_{\alpha\beta}Q_{\beta\alpha}\right)^2, \tag{3.4}$$

$$\begin{aligned} f_{elas} &= \frac{1}{3+2\kappa}\left[Q_{\alpha\beta,\gamma}Q_{\alpha\beta,\gamma} + \kappa Q_{\alpha\beta,\beta}Q_{\alpha\gamma,\gamma} + 4q_0\varepsilon_{\alpha\beta\gamma}Q_{\alpha\delta}Q_{\gamma\delta,\beta}\right. \\ &+ \left. 4q_0^2 Q_{\alpha\beta}Q_{\beta\alpha}\right]. \end{aligned} \tag{3.5}$$

Considering the constraints that the order parameter tensor is symmetric $Q_{\alpha\beta} = Q_{\beta\alpha}$, and traceless $Q_{\alpha\alpha} = 0$, we find the 5 Euler-Lagrange equations, one for each independent component of the order parameter tensor $Q_{\alpha\beta} = q_1, q_2, q_3, q_4, q_5$ (see Appendix B). We have assumed the one elastic constant approximation $\kappa = 0$.

$$-\nabla^2 q_1 - 2q_0\left[q_{2,z} - q_{3,y}\right] + 2q_0\left[-q_{2,z} + q_{3,y}\right] = -\omega\left[\Sigma q_1 - 6A_{11} + 2TrQ^2\right] \tag{3.6}$$

$$-\nabla^2 q_2 - q_0\left[-q_{1,z} + q_{3,x} + q_{4,z} - q_{5,y}\right] + q_0\left[q_{1,z} - q_{3,x} - q_{4,z} + q_{5,y}\right] = \\ = -\omega\left[\Sigma q_2 - 6A_{12}\right] \tag{3.7}$$

$$-\nabla^2 q_3 - q_0\left[2q_{1,y} - q_{2,x} + q_{4,y} + q_{5,z}\right] + q_0\left[-2q_{1,y} + q_{2,x} - q_{4,y} - q_{5,z}\right] = \\ = -\omega\left[\Sigma q_3 - 6A_{13}\right] \tag{3.8}$$

$$-\nabla^2 q_4 - 2q_0\left[-q_{2,z} + q_{5,x}\right] + 2q_0\left[q_{2,z} - q_{5,x}\right] = -\omega\left[\Sigma q_4 - 6A_{22} + 2TrQ^2\right] \tag{3.9}$$

$$-\nabla^2 q_5 - q_0\left[-q_{1,x} + q_{2,y} - q_{3,z} - 2q_{4,x}\right] + q_0\left[q_{1,x} - q_{2,y} + q_{3,z} + 2q_{4,x}\right] = \\ = -\omega\left[\Sigma q_5 - 6A_{23}\right] \tag{3.10}$$

with

$$\omega = \frac{6+4\kappa}{3} = 2 \tag{3.11}$$

$$\Sigma = \tau + \frac{4}{3}TrQ^2 + \frac{6}{3+2\kappa}q_0^2 = \tau + \frac{4}{3}TrQ^2 + 2q_0^2 \tag{3.12}$$

$$A_{11} = q_1^2 + q_2^2 + q_3^2 \tag{3.13}$$

$$A_{12} = q_1 q_2 + q_2 q_4 + q_3 q_5 \tag{3.14}$$

$$A_{13} = q_2 q_5 - q_3 q_4 \tag{3.15}$$

$$A_{22} = q_2^2 + q_4^2 + q_5^2 \tag{3.16}$$

$$A_{23} = q_2 q_3 - q_5 q_1. \tag{3.17}$$

The second step is to impose the cylindrical symmetry to the system. The procedure is detailed in Appendix B. It consists of writing the Euler-Lagrange equations in cylindrical coordinates (ρ, θ, z), eliminating the derivatives in θ by noticing that any semi-plane with fixed θ can be obtained by a rotation of the semi-plane with $\theta = 0$ around the z axis (chosen as the symmetry axis), and, finally, fixing a value for the angle θ. For simplicity, we have chosen $\theta = 0$ [46].

The 5 equations that we obtain for the cylindrical symmetry model are

$$- \left(\frac{\partial^2 q_1}{\partial \rho^2} + \frac{\partial^2 q_1}{\partial z^2}\right) - \left[\frac{1}{\rho}\frac{\partial q_1}{\partial \rho} + 2q_0\frac{\partial q_2}{\partial z}\right] + 2q_0\left[-\frac{\partial q_2}{\partial z}\right] = \\ - \omega\left[\Sigma q_1 - 6A_{11} + 2TrQ^2\right] + \frac{2}{\rho^2}\left(q_4 - q_1\right) + \frac{4}{\rho}q_0 q_5 \tag{3.18}$$

$$- \left(\frac{\partial^2 q_2}{\partial \rho^2} + \frac{\partial^2 q_2}{\partial z^2}\right) - \left[\frac{1}{\rho}\frac{\partial q_2}{\partial \rho} + q_0\left(-\frac{\partial q_1}{\partial z} + \frac{\partial q_3}{\partial \rho} + \frac{\partial q_4}{\partial z}\right)\right] + \tag{3.19}$$
$$+ \quad q_0\left[\frac{\partial q_1}{\partial z} - \frac{\partial q_3}{\partial \rho} - \frac{\partial q_4}{\partial z}\right] = -\omega\left[\Sigma q_2 - 6A_{12}\right] - \frac{4}{\rho^2}q_2 - \frac{2}{\rho}q_0 q_3$$

$$- \left(\frac{\partial^2 q_3}{\partial \rho^2} + \frac{\partial^2 q_3}{\partial z^2}\right) - \left[\frac{1}{\rho}\frac{\partial q_3}{\partial \rho} + q_0\left(-\frac{\partial q_2}{\partial \rho} + \frac{\partial q_5}{\partial z}\right)\right] + \tag{3.20}$$
$$+ \quad q_0\left[\frac{\partial q_2}{\partial \rho} - \frac{\partial q_5}{\partial z}\right] = -\omega\left[\Sigma q_3 - 6A_{13}\right] - \frac{1}{\rho^2}q_3 - \frac{4}{\rho}q_0 q_2$$

$$- \left(\frac{\partial^2 q_4}{\partial \rho^2} + \frac{\partial^2 q_4}{\partial z^2}\right) - \left[\frac{1}{\rho}\frac{\partial q_4}{\partial \rho} + 2q_0\left(-\frac{\partial q_2}{\partial z} + \frac{\partial q_5}{\partial \rho}\right)\right] \tag{3.21}$$
$$+ \quad 2q_0\left[\frac{\partial q_2}{\partial z} - \frac{\partial q_5}{\partial \rho}\right] = -\omega\left[\Sigma q_4 - 6A_{22} + 2TrQ^2\right] + \frac{2}{\rho^2}\left(q_1 - q_4\right)$$

$$- \left(\frac{\partial^2 q_5}{\partial \rho^2} + \frac{\partial^2 q_5}{\partial z^2}\right) - \left[\frac{1}{\rho}\frac{\partial q_5}{\partial \rho} + q_0\left(-\frac{\partial q_1}{\partial \rho} - \frac{\partial q_3}{\partial z} - 2\frac{\partial q_4}{\partial \rho}\right)\right] + \tag{3.22}$$
$$+ \quad q_0\left[\frac{\partial q_1}{\partial \rho} + \frac{\partial q_3}{\partial z} + 2\frac{\partial q_4}{\partial \rho}\right] = -\omega\left[\Sigma q_5 - 6A_{23}\right] - \frac{1}{\rho^2}q_5 + \frac{2}{\rho}q_0\left(q_1 - q_4\right)$$

We shift the values in the ρ axis by a distance R, $\rho \to \rho + R$. This ensures that the symmetry axis is at a distance R from the simulated domain. R represents the internal radius of curvature of our systems. In order to simulate the limit with no curvature, we set R to ∞. In this limit, we recover the equations in an XZ reference frame.

We use two kinds of cells: rectangular and circular. With the procedure described above, they correspond to cross-sections of a cylinder with a hole of radius R cut in the middle, and to a torus with internal radius R, respectively (see Fig. 3.1).

The Euler-Lagrange equations are introduced in the commercial software COMSOL to solve them numerically. We use the provided Backward Differentiation Formula (BDF) with a variable time step to solve the differential equations. We combine it with the linear system solver UMFPACK, a direct method for unsymmetric sparse systems that uses LU factorization. The mesh for the discretization of the space is chosen so that each element cannot be bigger than a few correlation lengths ξ. This gives a good resolution of the space, given that the equilibrium configurations do not include topological defects. In regions with very high curvature, where the elastic distortions are specially strong, the mesh is manually refined to increase the resolution. Two types of boundary conditions are used: free, and fixed

director at the boundary.

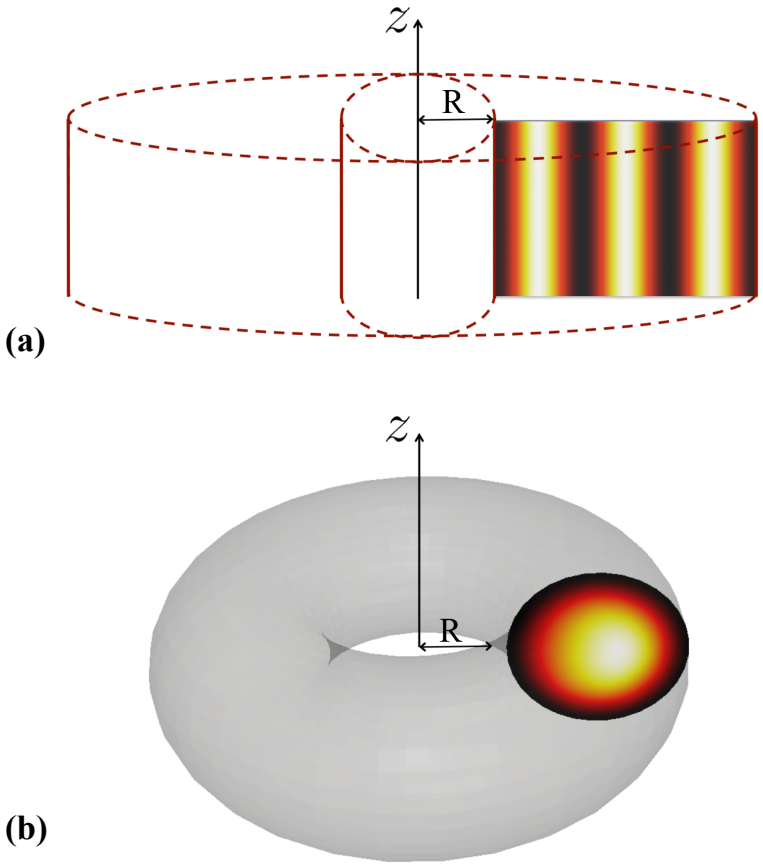

Figure 3.1: Schematic representation of the curved systems generated by considering rectangular and circular cells with imposed cylindrical symmetry around the z axis. (a) The rectangular cell represents a cross-section of an infinitely long cylinder with a cylindrical hole of radius R cut in the middle. (b) The circular cell represents a cross-section of a toroidal droplet with internal radius R.

3.2 Systems without cylindrical symmetry

For the three dimensional systems, we minimize the Laudau-de Gennes free energy using the Finite Element Method with Adaptive Meshing [45]. The minimization is calculated in several steps and the mesh is refined between each step. The domain is discretized by using the Quality Tetrahedral Mesh Generator, TetGen [47], library. In three dimensions the elements are tetrahedra. The values of the fields, *i. e.* of the independent components q_i of the order parameter tensor, are defined only at the nodes x_i of the mesh. The values of q_i at any other point $\mathbf{x}$ of the domain are calculated by a linear interpolation. The discretized integrals are evaluated

numerically using generalized Gaussian quadrature rules for multiple integrals [48]. The equilibrium values of the fields q_i at the vertices are obtained through numerical minimization. We use the INRIA's $M1QN3$ [49] optimization routine. The routine implements a limited-memory quasi-Newton technique (limited memory Broyden-Fletcher-Goldfarb-Shannon method) of Nocedal [50].

The boundary conditions result from the surface free energy (2.28), introduced in Chapter 2, that favours the planar degenerate alignment of the director at the surface of the droplet.

In between each minimization step, the mesh is refined in a way which is sensitive to the variation of the order parameter. In regions where the order parameter varies more abruptly, the mesh will be finer. The advantage of this method is that it optimizes the computing resources by using the minimal number of elements to meet the desired error tolerance and precision.

We achieve an energy precisions of order bellow 1%. However, reaching such a precision entails a high computational cost and it is, in many cases not necessary. In this thesis, we present configurations with precisions of the order of $1 - 10\%$. For all of them, we have verified that the details of the configuration do not suffer significant changes in the final minimization steps.

The highly confined cholesteric system may have many metastable configurations. We try to prevent the system from being arrested in metastable states by starting from the initial configuration in each step. We also keep track of the energy of each system in order to be able to compare competing configurations.

3.3 Visualization technique

From the minimization procedure we get the spacial profile of the tensorial order parameter. We visualize the configurations by plotting the orientation of the director as a field, and by calculating the projection of the director onto special directions.

We use the open-source software Paraview [51] for the visualization of the configurations. This software allows us to do simple calculations with the data defining the configuration, represent the director field, draw isosurfaces, and adjust the resolution of the representation. Figure 3.2 shows a snapshot of the Paraview command window.

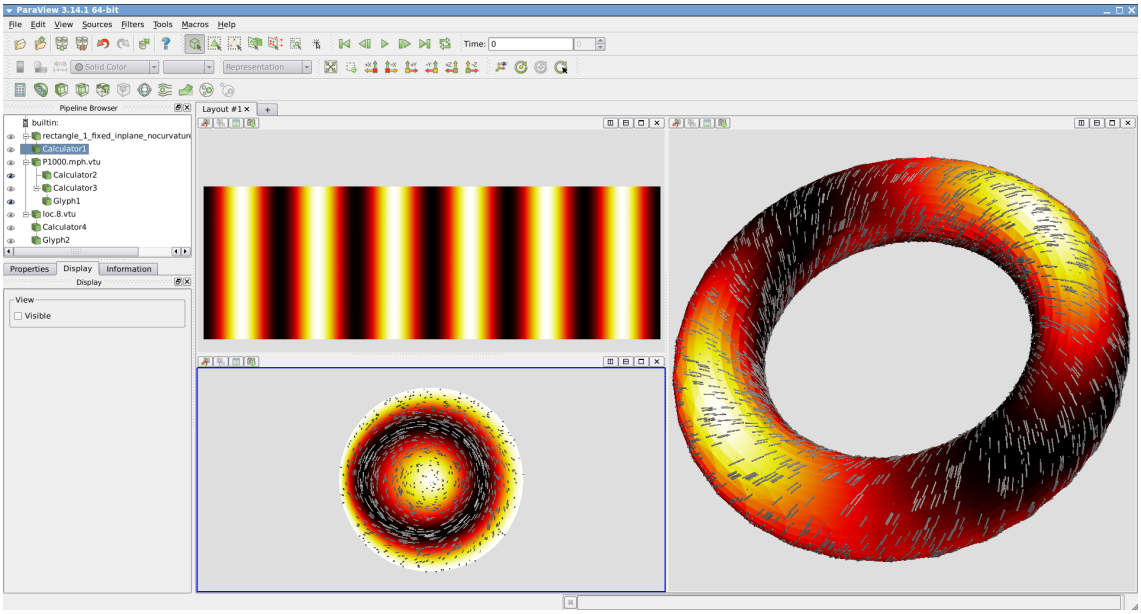

Figure 3.2: Visualization of the equilibrium cholesteric configurations with the Paraview software.

Chapter 4

Cholesteric Confined by Curved Surfaces

The main purpose of our study is to address the behaviour of a cholesteric confined inside a toroidal droplet. Liquid crystal droplets with toroidal shape have been produced in recent experiments [30], triggering a strong scientific interest in the resulting configurations.

Because the Euler characteristic of the torus is zero, this geometry has the distinctive property of imposing a net topological charge equal to zero on the director field of the cholesteric. This is stated by the Poincaré-Hopf theorem for any configuration in which the anchoring to the surface of the torus is planar [43]. As a result, the possible configurations for the system either present defects with symmetric topological charges or no defects at all.

Focusing on the defect-free configurations, one can study how curvature and confinement affect the texture, without considering any distortions due to defects. Such distortions would be unavoidable in other curved systems, like the sphere or the spherical shell [18]. It is the decoupling between curvature effects and topological constraints that renders the toroidal shape particularly interesting from a fundamental point of view.

The geometry of the torus is a complex one as it involves two different curvatures, one defines the circular cross-section and another refers to the bending around the symmetry axis. Thus, it is necessary to introduce two different curvature radii to characterize it. The choice of how to define these radii is not unique. In our work we have adopted to describe the torus by defining the radius of the cross-section r and the internal radius of the torus R (see Fig. 4.1). Such choice was made in order to facilitate the comparison with other geometries presented in the chapter.

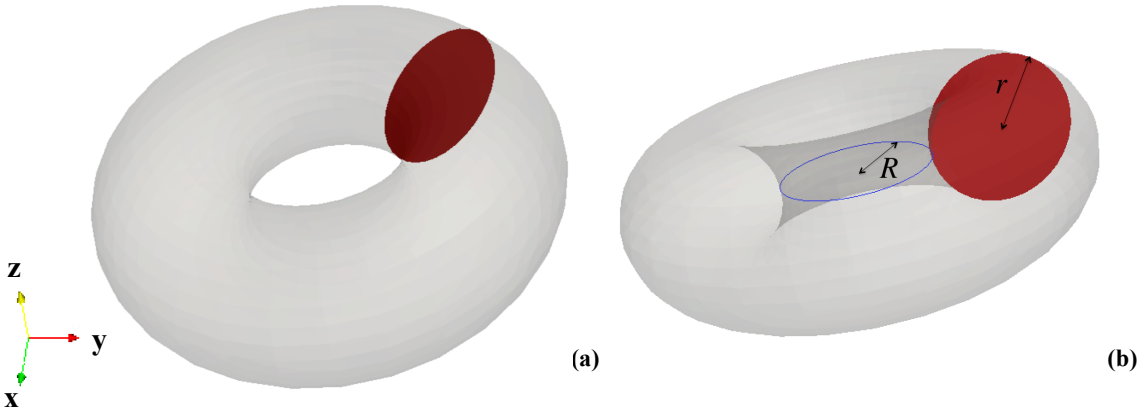

Figure 4.1: (a) The toroidal shape with circular cross-section drawn in red. (b) Definition of the radii for the torus. Radius of the cross-section r and internal radius of the torus R.

Given the intrinsic complexity of the toroidal geometry, we try to analyse separately the effects of the two curvatures. To this end, we target three different geometries, which are successively more complex, in order to approach the characteristics of the torus.

In this chapter we present and examine the obtained configurations for the cholesteric liquid crystal confined inside the three curved systems. We show how the curvature influences the orientation of the director field close to the boundary and how this affects the equilibrium configurations for each system. The curvature of the confining surface introduces distortions in the natural periodicity of the cholesteric that depend on the director's orientation. For systems in which the only constraint arises from one curved wall, the result is a spatially modulated cholesteric pitch that depends on the distance to the centre of curvature (Section 4.1). In systems with further constraints (Sections 4.2 and 4.3), we observe a symmetry break in the cholesteric configurations, with the equilibrium state depending on the relative orientation of the director at the boundary.

4.1 Cholesteric close to a curved wall

The system presented in this section is a two-dimensional rectangular cell of dimensions $L \times h$, which is filled with cholesteric liquid crystal. The rectangular cell represents a cross-section of the three-dimensional system shown in Fig. 4.2, for which rotational invariance is assumed. The distance R between the limit of the cell and the axis of rotation is the radius of curvature of the interior wall. We are particularly interested in the behaviour of the cholesteric close to this curved wall. Also,

we want to determine if the effects of the curvature are local or if they propagate to the entire system.

Note that the curvature considered is analogous to the internal curvature of the torus. This study is the first approximation to the investigation of the toroidal droplet.

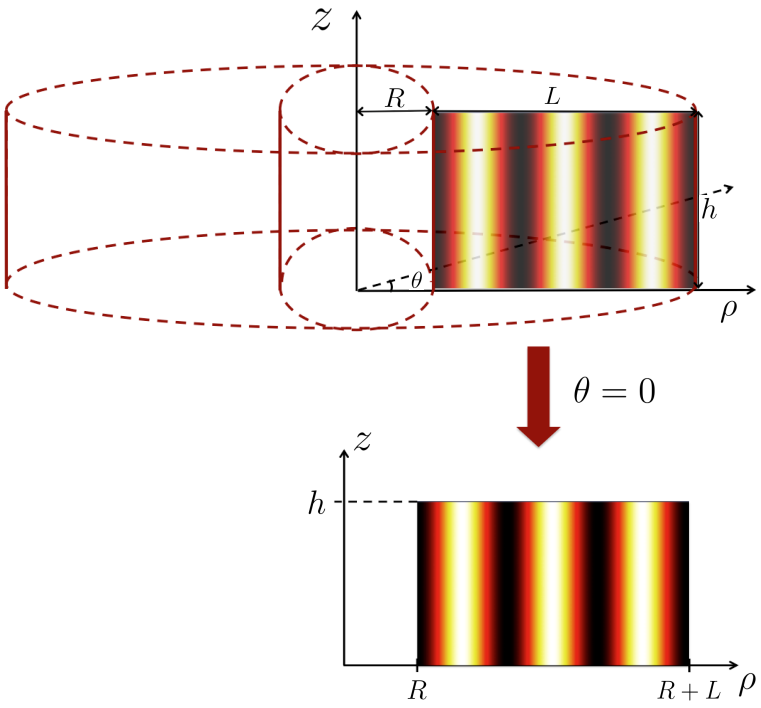

Figure 4.2: Scheme of the system simulated by considering a $L \times h$ rectangular cross-section and imposing cylindrical symmetry around the z-axis, which is a distance R away from the rectangular cell.

The dimensions of the cell are defined in the scale of the correlation length of the colesteric. We fix the size of the cell to $L = 3000\xi$ and $h = 1000\xi$. The system is then completely defined by the Euler-Lagrange equations corresponding to the Landau-de Gennes free energy and by the initial and boundary conditions. We assume periodic boundary conditions for the top and bottom of the box so that an infinite system is simulated in the direction parallel to the symmetry axis. On the left lateral boundary, the conditions are of fixed director, either parallel to the symmetry axis or perpendicular to plane of the cross-section. This allows us to investigate how the preferred orientation close to a curved surface affects the rest of the configuration. For the right lateral boundary, both fixed director and free conditions are considered. Switching between fixed and free conditions, corresponds to having a constant or variable number of cholesteric layers, respectively. The initial conditions consist of a cholesteric twisting around an horizontal axis with its unperturbed pitch P_0. The

two values of P_0 chosen for this simulation are $P_0 = 1000\xi$ and $P_0 = 500\xi$, both of them commensurable with the lenght L of the system.

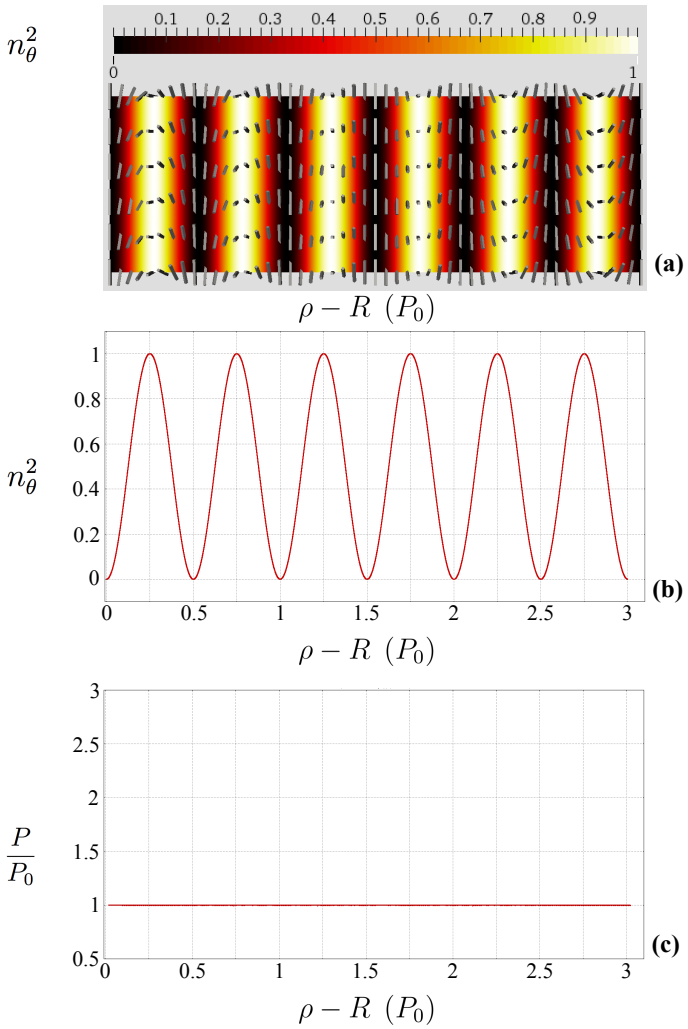

Figure 4.3: Initial conditions. (a) Configuration of cholesteric with twist along the horizontal direction. The color corresponds to the values of n_θ^2 and the grey bars represent the director field. (b) Plot of n_θ^2 along an horizontal line. c) Plot of $\frac{P}{P_0}$ along an horizontal line. The distances are in units of the natural pitch of the cholesteric P_0.

Figure 4.3 is a representation of the initial conditions with $P_0 = 1000\xi$. In the first image (Fig. 4.3 (a)), the color scale is relative to the square of the component n_θ of the director (the component perpendicular to the cross-section). The grey bars represent the director field. Figure 4.3 (b) presents n_θ^2 along the horizontal direction, while Fig. 4.3 (c) shows the values of the pitch relative to the natural pitch of the cholesteric, $\frac{P}{P_0}$, along the same horizontal line. The values of $\frac{P}{P_0}$ are obtained through the calculation of the twist parameter S_{tw} [52, 32] (see Appendix

C for the relation between S_{tw} and the ratio $\frac{P}{P_0}$). All the configurations in this section will be analysed on the basis of these three types of plot. In Fig. 4.3 for the initial conditions, the cholesteric layers are undistorted, with n_θ^2 varying in a sinusoidal fashion and $\frac{P}{P_0}$ being always constant and equal to 1.

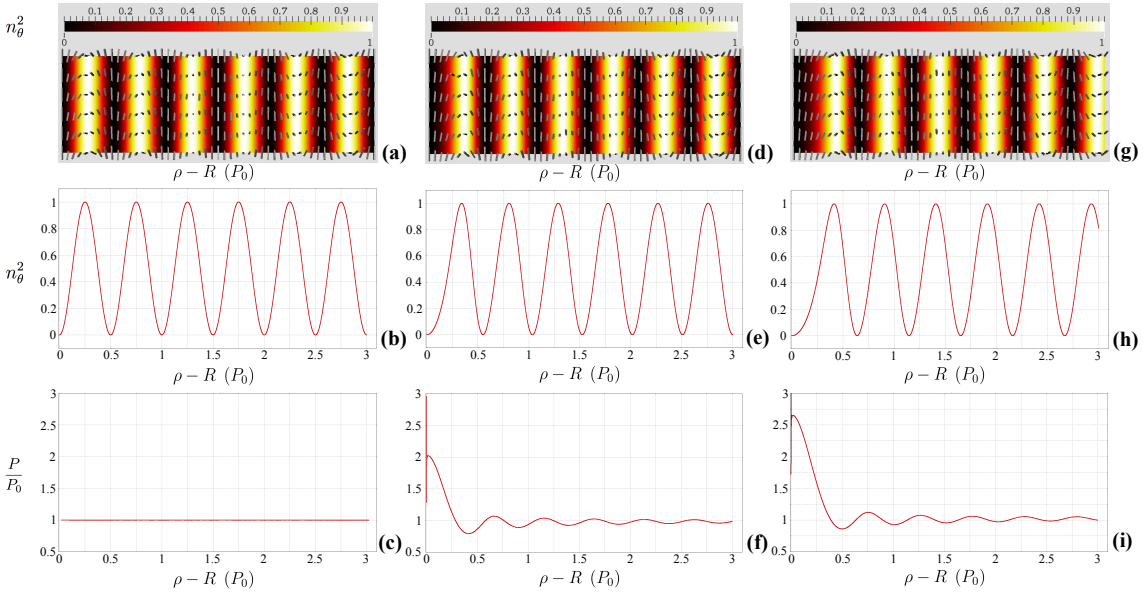

Figure 4.4: Comparison of the equilibrium configurations of the systems with no curvature, with curvature ($R = 1\xi$) and fixed outer boundary, and with curvature ($R = 1\xi$) and free outer boundary, for $P_0 = 1000\xi$. (a), (b), and (c): equilibrium configuration in the no curvature limit $R \to \infty$. (d), (e), and (f): equilibrium configuration for a system with radius of curvature $R = 1\xi$ and fixed outer boundary. (g), (h), and (i): equilibrium configuration for a system with radius of curvature $R = 1\xi$ and free outer boundary. (a), (d), and (g) show the cholesteric configuration. The color scale refers to n_θ^2 and the grey bars represent the director field. (b), (e), and (h): value of n_θ^2 along an horizontal line. (c), (f), and (i): ratio between the local pitch and the natural pitch of the cholesteric along an horizontal line. The distances are in units of the natural pitch of the cholesteric P_0.

When the curvature is introduced and the system is allowed to relax to its equilibrium configuration, we observe distortions in the twist of the cholesteric. The pitch is no longer spatially uniform. Figure 4.4 shows the effect. The simulation was made for three different systems, all starting from the initial configuration showed in Fig. 4.3 with $P_0 = 1000\xi$. For the three systems, the conditions on the left boundary were of fixed director parallel to the symmetry axis (see Fig. 4.2). Figure 4.4 (a), (b) and (c) show the results for a system with no curvature, obtained by taking the limit $R \to \infty$ in the Euler-Lagrange equations. Fig. 4.4 (d) to (i) correspond to a very high curvature with radius $R = 1\xi$. For Fig. 4.4 (d), (e) and (f) the right boundary is also fixed with director parallel to the symmetry axis and for Fig. 4.4

(g), (h) and (i) the right boundary was left free.

The result for the system with no curvature is identical to the initial condition, with constant pitch $P = P_0$ (see Fig. 4.4 (a) to (c)). Elastic deformations appear only in systems with finite curvature radius R (see Fig. 4.4 (d) to (i)). Therefore, we conclude that the distortions are a consequence of the curvature.

Such distortions can be described as an increase of the length of the regions where the director is parallel to the symmetry axis ($n_\theta = 0$) and a decrease of the length of the regions where the director has a component on the plane perpendicular to it. This, in turn, corresponds to an increase of the pitch for the first case and a decrease of the pitch for the latter (see Fig. 4.4 (f) and (i)).

The distortions just described are a way of minimizing the additional elastic energy that appears due to the curvature. This elastic energy depends on the local orientation of the director. Because the liquid crystal must follow the curvature of the system, there is only one orientation for which there is no energy increase. If the director is pointing vertically along $\mathbf{e}_z$, *i.e.*, parallel to the symmetry axis, the curvature does not imply any additional distortion. Therefore, in that case, there is no additional energy cost. However, if the director has a component on the plane perpendicular to the symmetry axis, the elastic energy increases. Any component along $\mathbf{e}_\theta$ is made to bend because of the curvature. Components along $\mathbf{e}_\rho$ correspond to a splay deformation.

As a result, the preferred local orientation of the director is parallel to the symmetry axis. Thus, regions with such orientation tend to extend. However, there is an energy cost associated with the distortion of the twist natural periodicity. How much the cholesteric layers are distorted in the equilibrium configuration is a result of the competition between the bend and splay elastic energies, and the energy of distorting the natural cholesteric pitch.

Because the elastic energy increases with the curvature, the strength of the distortions varies in space. The maximum of the distortion is on the first layer from the wall. In this region, the bend and splay elastic energies are much higher than the cholesteric term. As the distance from the curved wall increases, the elastic energy cost decreases and the cholesteric energy term starts to dominate. As a result, The value of $\frac{P}{P_0}$ is maximum in the layer which is closest to the wall and diminishes with the increase of $\rho - R$, while oscillating between parallel and perpendicular cholesteric layers (see Fig. 4.4 (f) and (i)).

The distortions are stronger for the system with less constraints, the one with a free right boundary (compare Fig. 4.4 (h) and (i) with Fig. 4.4 (e) and (f)). This is justified because the system is able to release the stress by changing the number

of cholesteric layers inside the cell.

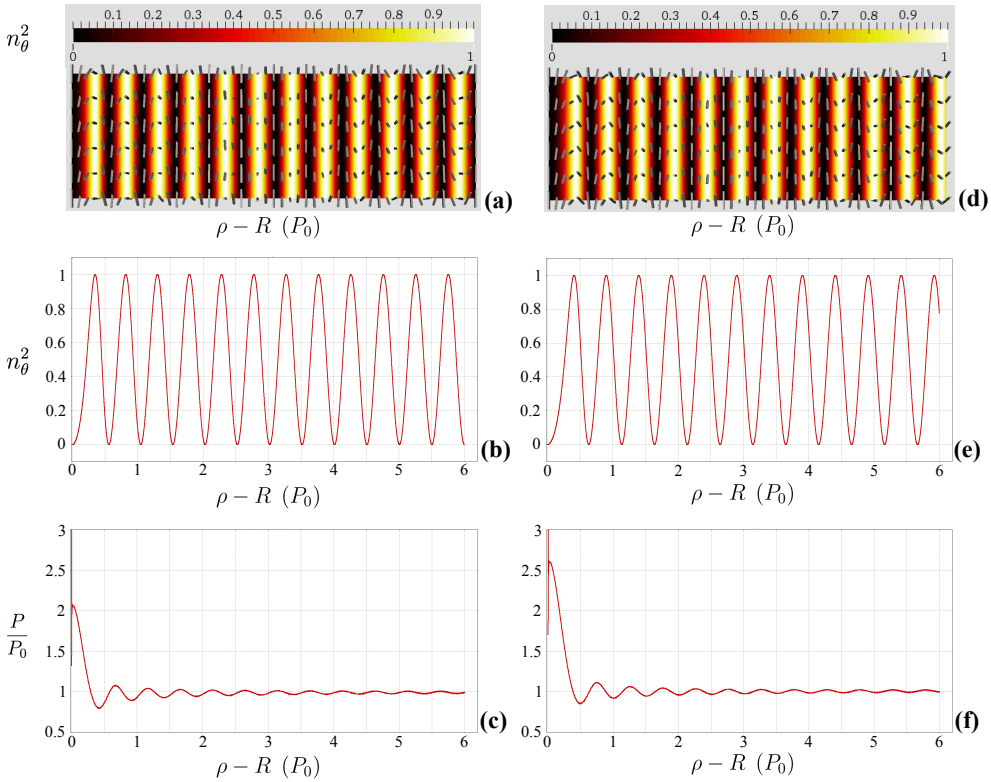

Figure 4.5: Equilibrium configurations for systems with a natural pitch $P_0 = 500\xi$ and curvature radius $R = 1\xi$. (a), (b), and (c): fixed outer boundary. (d), (e), and (f): free outer boundary. (a) and (d) show the cholesteric configuration. The color scale refers to n_θ^2 and the grey bars represent the director field. (b) and (e): value of n_θ^2 along an horizontal line. (c) and (f): ratio between the local pitch and the natural pitch of the cholesteric $\frac{P}{P_0}$ along an horizontal line. The distances are in units of the natural pitch of the cholesteric P_0.

The results do not depend on the cholesteric natural pitch. The same pattern of periodic layer deformations, decreasing with the distance from the wall is observed for $P_0 = 500\xi$ (see Fig. 4.5). The effect is also more pronounced for the system with the free outer boundary. The maximum value for the variation of the pitch $\frac{P}{P_0}$ is the same as in the previous system with $P_0 = 1000\xi$.

On the other hand, an increase of the the radius of curvature R leads to a decrease in the strength of the distortions. Figure 4.6 shows plots of the variation of $\frac{P}{P_0}$ with the distance to the curved surface for four different values of R, $R = 10\xi, 100\xi, 250\xi, 1000\xi$. The maximum value of $\frac{P}{P_0}$ and the amplitude of the subsequent oscillations both decrease with the increase of the curvature radius.

These results suggest that the preferred configuration for a cholesteric close to a curved convex wall is the one in which the director points parallel to the axis

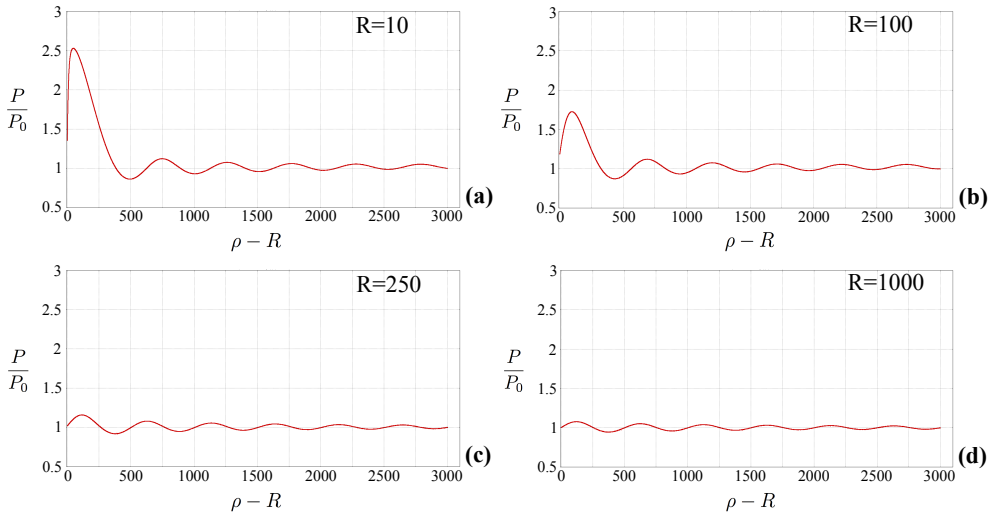

Figure 4.6: Variation of $\frac{P}{P_0}$ with the distance to the symmetry axis for different values of the curvature: (a) $R = 10\xi$, (b) $R = 100\xi$, (c) $R = 250\xi$, and (d) $R = 1000\xi$. The distances are in units of the natural pitch of the cholesteric P_0.

of rotation. This is combined with the twisting of the cholesteric by expanding the regions with such orientation, a distortion effect which is stronger for higher curvatures. To further support this observation, we performed simulations in which the conditions on the boundary with higher curvature are of fixed director along $\mathbf{e}_\theta$. It is our conjecture that this kind of configuration will be highly unstable due to a great increase in energy from bending. Figure 4.7 shows the minimized configurations for this kind of boundary conditions, natural pitch $P_0 = 1000\xi$, and radii of curvature $R = 1\xi, 50\xi, 100\xi$.

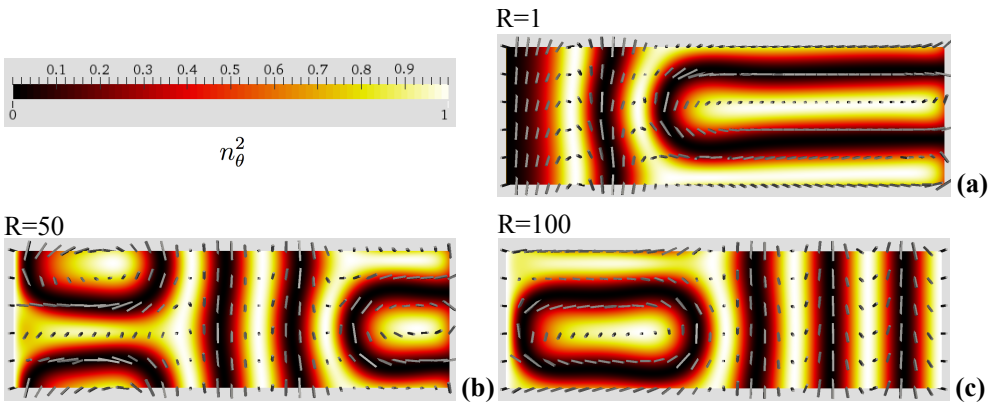

Figure 4.7: Cholesteric configurations obtained for systems with fixed boundary conditions of director parallel to $\mathbf{e}_\theta$ on the inner boundary. Natural pitch $P_0 = 1000\xi$. (a) Curvature radius $R = 1\xi$. (b) $R = 50\xi$. (c) $R = 100\xi$. The color scale refers to n_θ^2 and the grey bars represent the director field.

The configurations obtained are considerably more complex, with the direction of twist also varying in space. A closer look at the regions near the wall reveals that the system has two different ways of minimizing the elastic energy. For smaller curvatures, $R = 50\xi, 100\xi$ (see Fig. 4.7 (b) and (c)), the direction of the twist is altered. The system twists in the direction parallel to the symmetry axis. Because the system is twisting along that direction, the region with disfavoured orientation is decreased to a small fraction of the height of the cell. For a very high curvature, $R = 1\xi$ (see Fig. 4.7 (a)), there is a sudden change in the orientation. The system assumes the preferred orientation very close to the wall. This implies very high energy cost for distorting the natural pitch periodicity. However this is still lower that the elastic energy cost for such a high curvature.

4.2 Toroidal droplet with imposed axial symmetry

The preferred orientation of the cholesteric director close to a curved wall is parallel to the axis of rotation. This orientation allows the molecules to follow the curvature of the system without undergoing any elastic distortions. Keeping this conclusion in mind, we increase the confinement of the system, moving up one step in the complexity ladder.

In the present section, we substitute the rectangular cell by a circular one, with radius r. It is our purpose to understand how the system will accommodate to the addition of a second confinement by a second curved surface. The model used is the same as in Section 4.1, meaning that the circular cell represents a $\theta = 0$ cross-section of a three-dimensional system with cylindrical symmetry. Thus, the corresponding system, generated by the revolution of the circular cross-section around the z axis, is a torus with imposed cylindrical symmetry. Just like before, the left edge of the cell is at a distance R from the axis of symmetry (and the centre of the circle is at a distance $R+r$). R is the internal radius of the torus. Unlike what happened for the rectangular cell, each point of the boundary is at a different distance from the axis of symmetry and experiences a different Gauss curvature. We expect the effects of curvature to be particularly noticeable in the surroundings of the point closer to the z-axis, which is the left extremity of the horizontal diameter.

In our simulations, we use two types of fixed boundary conditions: i) director pointing along the direction $\mathbf{e}_\theta$, locally parallel to the curvature with radius R (and perpendicular to the cross-sectional plane), and ii) director locally parallel to the circle (on the plane of the cross-section). These conditions are indexed by an angle ϕ, ϕ is the angle between the director on the boundary and the $\mathbf{e}_\theta$ direction. $\phi = 0$

corresponds to condition i) and $\phi = \frac{\pi}{2}$ corresponds to condition ii). Isotropic initial conditions were used in the simulations since an aligned initial condition would be a metastable configuration for fixed boundary conditions in the same direction.

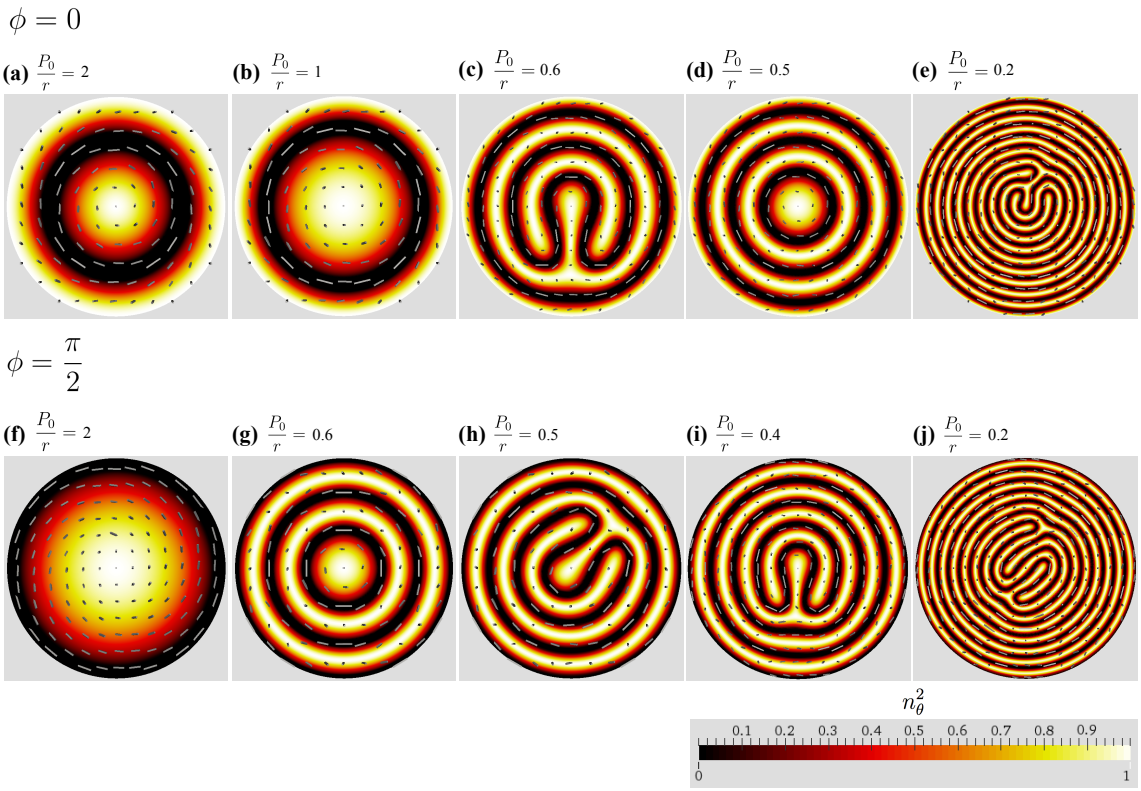

Figure 4.8: Equilibrium configurations for a cholesteric liquid crystal inside an infinite cylinder with radius $r = 500\xi$. (a) to (e): fixed boundary conditions with director parallel to the long axis of the cylinder (z-axis). (f) to (j) fixed boundary conditions with director tangent to the limiting circumference, on planes of constant z. The color represents n_θ^2, the square of the component of the director along $\mathbf{e}_\theta$. The grey bars represent the director field.

Figure 4.8 shows the equilibrium configurations for the no curvature limit with a radius of cross-section $r = 500\xi$ and varying natural pitch P_0. To better understand the dimensions of the systems, they will be labelled by the ratio $\frac{P_0}{r}$. The results shown correspond to fixed boundary conditions with director perpendicular to the disk (i), and parallel to the circumference (ii).

The no curvature limit $R \to \infty$ corresponds, for the circular cross-section, to an infinite cylinder . We chose the cylinder as a starting point in order to consider again only one curvature, which is the simpler case. The configurations of a cholesteric liquid crystal inside a cylinder have already been studied [31, 32]. Among the equilibrium configurations that were observed, a radial configuration is documented. In this configuration the twist occurs along the radial directions, giving origin to a

pattern of circular concentric cholesteric layers. This configuration was found to be persistent in our simulations.

In Fig. 4.8, we observe the radial-like configuration, with the centre of the concentric layers coinciding with the centre of the circle. Some of the values of r and P_0 are not commensurable for the corresponding boundary conditions, resulting in configurations with distorted layers. The system accommodates this incommensurability in two ways, one is to have a non-uniform pitch, resulting in layers with different lengths, the other is to have incomplete or reentrant layers, exhibiting a fingerprint like texture.

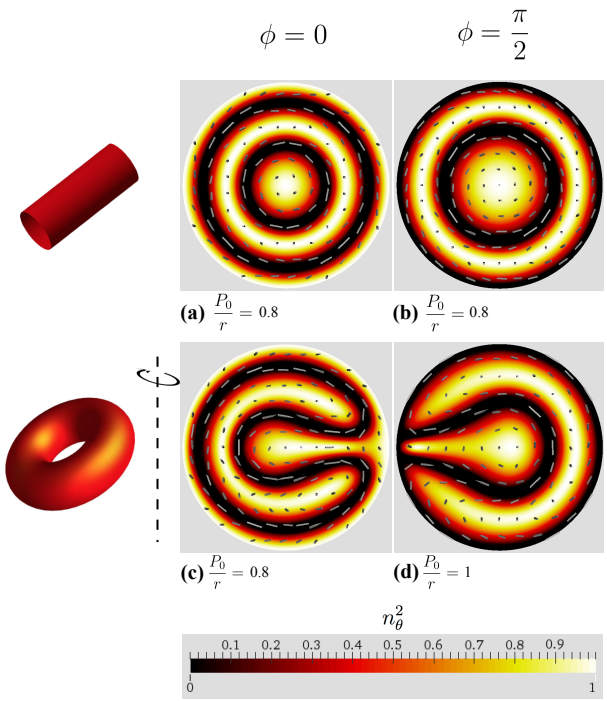

Figure 4.9: Comparison between the cholesteric configurations for the no curvature limit ((a) and (b)) and for a curvature radius $R = 50\xi$ ((c) and (d)). Systems (a) and (c) have boundary conditions with $\phi = 0$ and systems (b) and (d) have $\phi = \frac{\pi}{2}$. The color represents n_θ^2, the square of the component of the director along $\mathbf{e}_\theta$. The grey bars represent the director field.

We did not find other types of configurations for this system. It is possible that the reason for the persistence of the radial-like configuration, even when the dimensions are incommensurable, is the use of fixed boundary conditions. Starting from the isotropic initial condition, the cholesteric phase starts to align at the boundary and develops its twist from there towards the centre of the cylinder, adjusting for the incommensurability along the way.

The radial configuration is a starting point for the investigation of the effects of

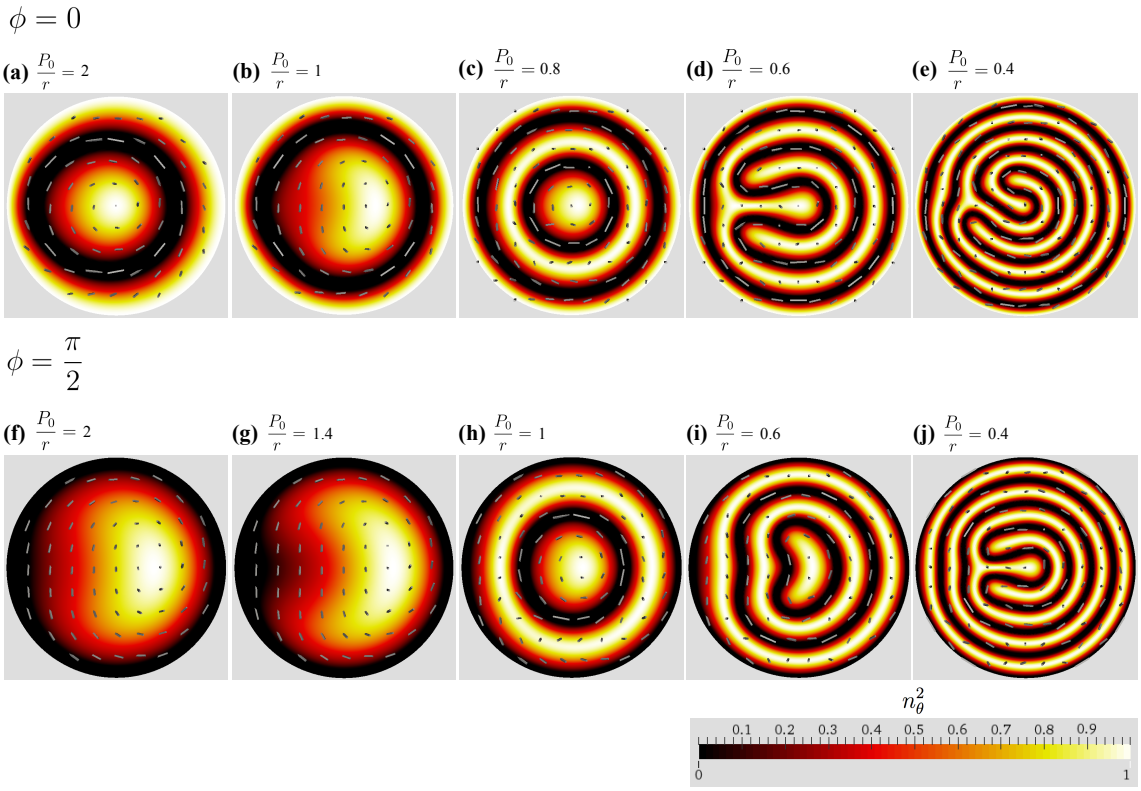

Figure 4.10: Cholesteric configurations for a system with radius of curvature $R = 50\xi$. (a) to (e) correspond to boundary conditions with $\phi = 0$, and (f) to (j) have boundary conditions with $\phi = \frac{\pi}{2}$. The color represents n_θ^2, the square of the component of the director along $\mathbf{e}_\theta$. The grey bars represent the director field.

the curvature in distorting the cholesteric layers. Let us now analyse the situation in which the curvature is present. We have used a curvature radius $R = 50\xi$. Smaller curvature radii, like the ones used in Section 4.1, increase the tendency for singularities in the orientational field, given that this is a much more constrained system. We try to avoid these singularities in order to focus on the pure elastic effects. Figure 4.9 shows the comparison between the configurations with and without curvature for both boundary conditions. The curvature introduces a symmetry breaking from the concentric layers observed in the cylinder.

The orientation of the layers in the curved system depends on the boundary orientation and it is such that in the system with $\phi = 0$ the region with the same orientation as the boundary is expanded close to the left boundary, and in the system with $\phi = \frac{\pi}{2}$ the region with the boundary orientation is contracted. This results in the packing of the layers observed in Fig. 4.9 (c) and (d).

This observation corroborates the previous findings that the preferred orientation in the regions of higher curvature is parallel to the symmetry axis z. We believe

that it is the high elastic energy cost for the regions with higher curvature that causes the symmetry break and the shift of the centre of the layers. This will be the main argument when analysing the three-dimensional configurations in Section 4.3. For further examples of cholesteric configurations whose layers are distorted due to curvature see Fig. 4.10. The configurations observed are very similar to the ones in Fig. 4.8 for the cylinder limit. The twist of the colesteric is along the radial directions and in Fig. 4.10 (d), (e), (h), (i), and (j) we see a fingering texture. However, the layers are distorted in comparison to the cylinder ones. This effect is more visible on the left side, which is closer to the boundary with higher curvature. For the configurations with $\phi = 0$ the cholesteric layers seem to move closer to the boundary because the extension of the region with $n_\theta = 1$ is decreased. On the contrary, for the configurations with $\phi = \frac{\pi}{2}$ the cholesteric layers seem to move away from the boundary because the extension of the region with $n_\theta = 0$ is increased.

4.3 Toroidal droplet with planar degenerate anchoring

In this Section, the constraint of cylindrical symmetry for the torus is lifted. Therefore, a fully three-dimensional toroidal droplet is simulated. We use the planar degenerate anchoring described in Chapter 2. The director on the boundary is parallel to the surface but it is free to point in any direction on it. In particular, the director can point in different directions for sections with different values of θ, therefore breaking the cylindrical symmetry. The anchoring is strong, with an anchoring constant $W = 0.01 J/m^2$. The system is now less constrained and the director can vary its alignment on the surface in order to minimize elastic distortions.

The configuration used for the initial conditions is one of a nematic aligned along the torus. This mimics the experimental set-up, where the droplet is produced by pushing the liquid crystal through a needle. The flow alignment corresponding to this procedure should induce a configuration with the director field aligned along the torus.

The obtained profiles are observed on the surface and inside the toroidal droplet. Figure 4.11 shows three toroidal systems with different dimensions. Inside the droplet, we observe that the twist is in the radial directions, just like in Section 4.2. The line in white in the centre of the droplet (see Fig. 4.11 (b) and (d)) represents a region where the director points along $\mathbf{e}_\theta$. Without the escape into the third dimension, this line would be a topological defect. This situation is referred to in the literature as a non-singular defect and occurs mostly in cholesterics due

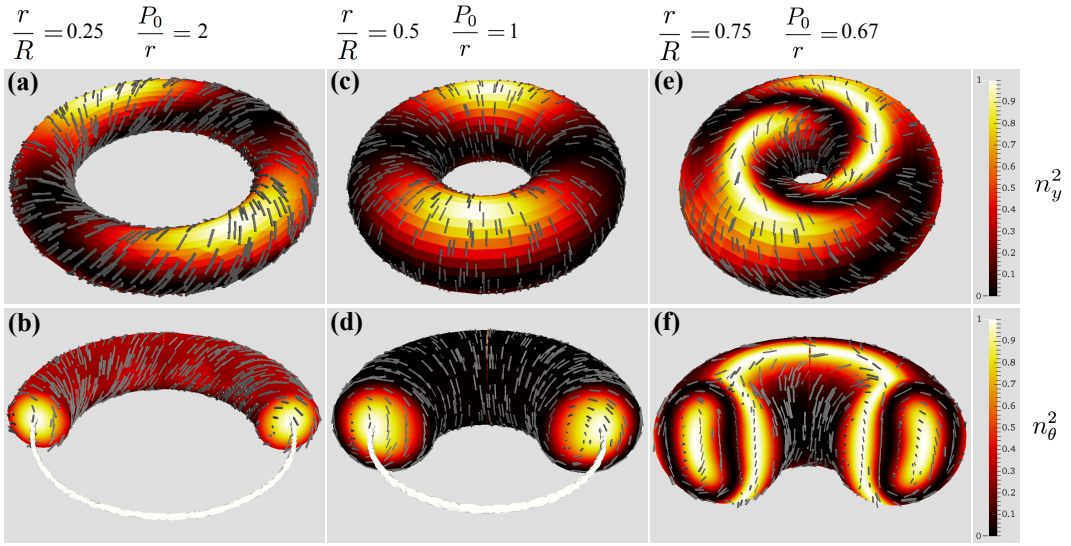

Figure 4.11: Equilibrium configurations for a toroidal droplet with planar degenerate anchoring on the surface. (a) and (b): $\frac{r}{R}=0.25$, $\frac{P_0}{r}=2$. (c) and (d): $\frac{r}{R}=0.5$, $\frac{P_0}{r}=1$. (e) and (f): $\frac{r}{R}=0.75$, $\frac{P_0}{r}=0.67$. (a), (c) and (e): orientation on the surface. The color refers to the square of the component of $\mathbf{n}$ along $\mathbf{e}_y$, n_y^2, and the grey bars represent the director field. (b), (d) and (f): orientation inside the droplet. The color scale refers to the square of the component of $\mathbf{n}$ along $\mathbf{e}_\theta$, n_θ^2, and the grey bars, again, represent the director field. The white line on the centre of the torus in (b) and (d) represents a non-singular defect where the director escapes to the direction perpendicular to the cross-section.

to the spontaneous twist in the third direction. On the surface of the droplet, the configuration is twisted in two of the systems (see Fig. 4.11 (a) and (e)). However, one of the systems (see Fig. 4.11 (c)) exhibits a surface configuration where the director is on the plane of the cross-section, resulting in cylindrical symmetry. This is a result of the commensurability between the natural pitch of the cholesteric and the radius of the cross-section of the torus. Fig. 4.13 (c) shows another example.

We should also note that, in many systems, we find configurations where the cholesteric layers are concentric. It was already expected that the effect of the curvature for the three-dimensional toroidal droplet was less intense than for the systems with imposed cylindrical symmetry, since the former is a system with less constraints. This fact, together with a smaller curvature, results in undistorted layers for some systems.

A twisted configuration had already been found for a toroidal droplet filled with nematic liquid crystal in the experimental study performed in [30]. However, the reason presented for the twisted nematic configurations is the presence of the elastic term K_{24} which is not considered in our equations. We further investigate the

nematic limit by increasing the pitch of the cholesteric (see Fig. 4.12). We find that the configurations for very high pitch have the director aligned along the torus. This supports the conjecture that there is some element missing in the model to fully describe the nematic system. However, the reason for the twist observed in the cholesteric configurations is a different one, most likely the natural pitch of the cholesteric.

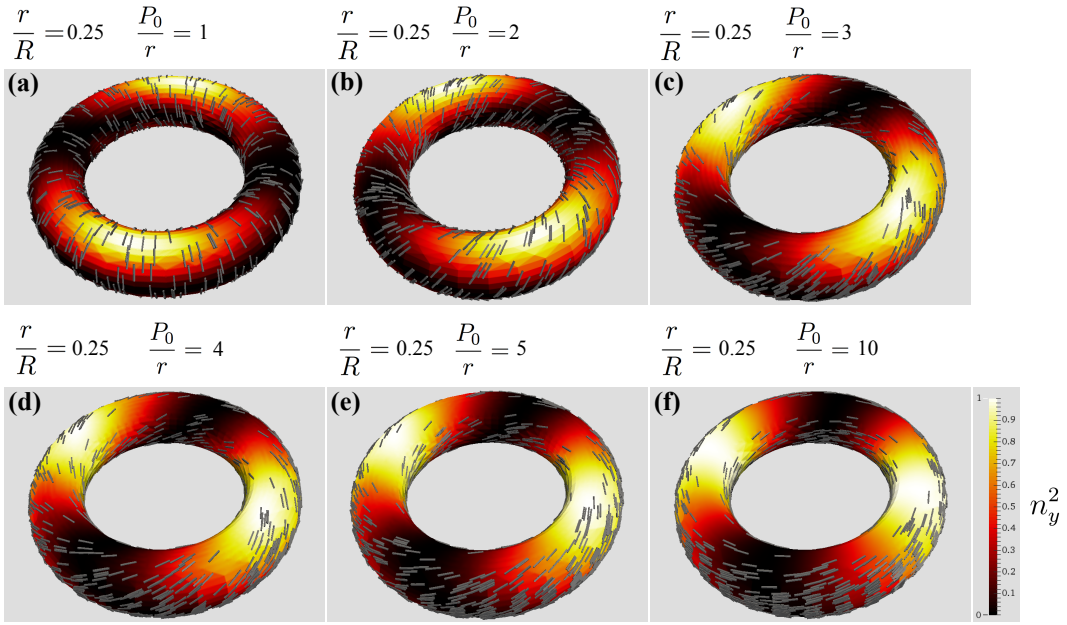

Figure 4.12: Surface configurations of a cholesteric inside a toroidal droplet with increasing natural pitch P_0. $\frac{r}{R}=0.25$ and (a) $\frac{P_0}{r}=1$, (b) $\frac{P_0}{r}=2$, (c) $\frac{P_0}{r}=3$, (d) $\frac{P_0}{r}=4$, (e) $\frac{P_0}{r}=5$, (f) $\frac{P_0}{r}=10$. The color scale refers to n_y^2 and the grey bars represent the director field.

To investigate the distortions caused by the curvature on the cholesteric layers, we simulate systems with a smaller pitch so that more layers can be formed. It is important to note that because the director is free to point in any direction on the surface, there is no constraint that the cholesteric layers have to be closed. The energy that results from elastic distortions on the surface has a lower value than the energy of distorting the periodicity of the cholesteric. Therefore, the preferred way of accommodating the incommensurability is to have distortions on the surface. Figure 4.13 shows three of these systems. Although the effects of the curvature are more subtle in the less constrained system, we observe that the packing of the layers is very similar to the one found in Section 4.2 for the $\phi=\frac{\pi}{2}$ boundary condition. This can be explained by noting that the orientation parallel to the vertical axis on the surface with higher curvature allows to minimize the elastic energy in these regions. As a matter of fact, in the inner region of the torus, the director almost

always points parallel to the vertical axis. This effect is higher when the curvature is higher (see Fig. 4.14).

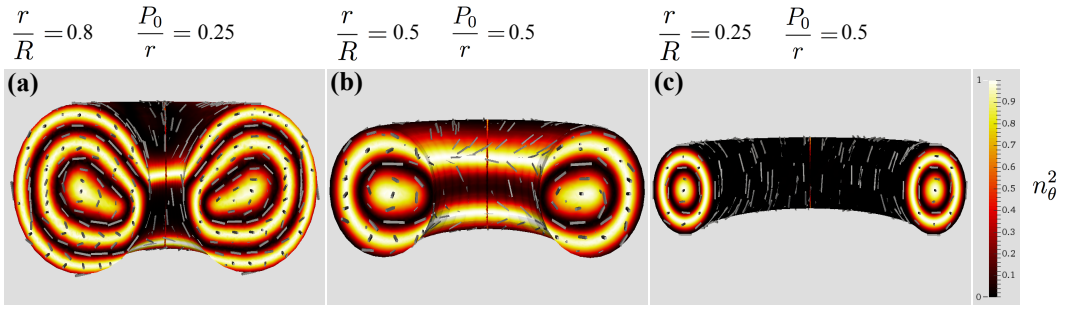

Figure 4.13: Configurations of a cholesteric inside a torus, with multiple layers. (a) $\frac{r}{R}=0.8$, $\frac{P_0}{r}=0.25$, (b) $\frac{r}{R}=0.5$, $\frac{P_0}{r}=0.5$, (c) $\frac{r}{R}=0.25$, $\frac{P_0}{r}=0.5$. The color scale refers to n_θ^2 and the grey bars represent the director field.

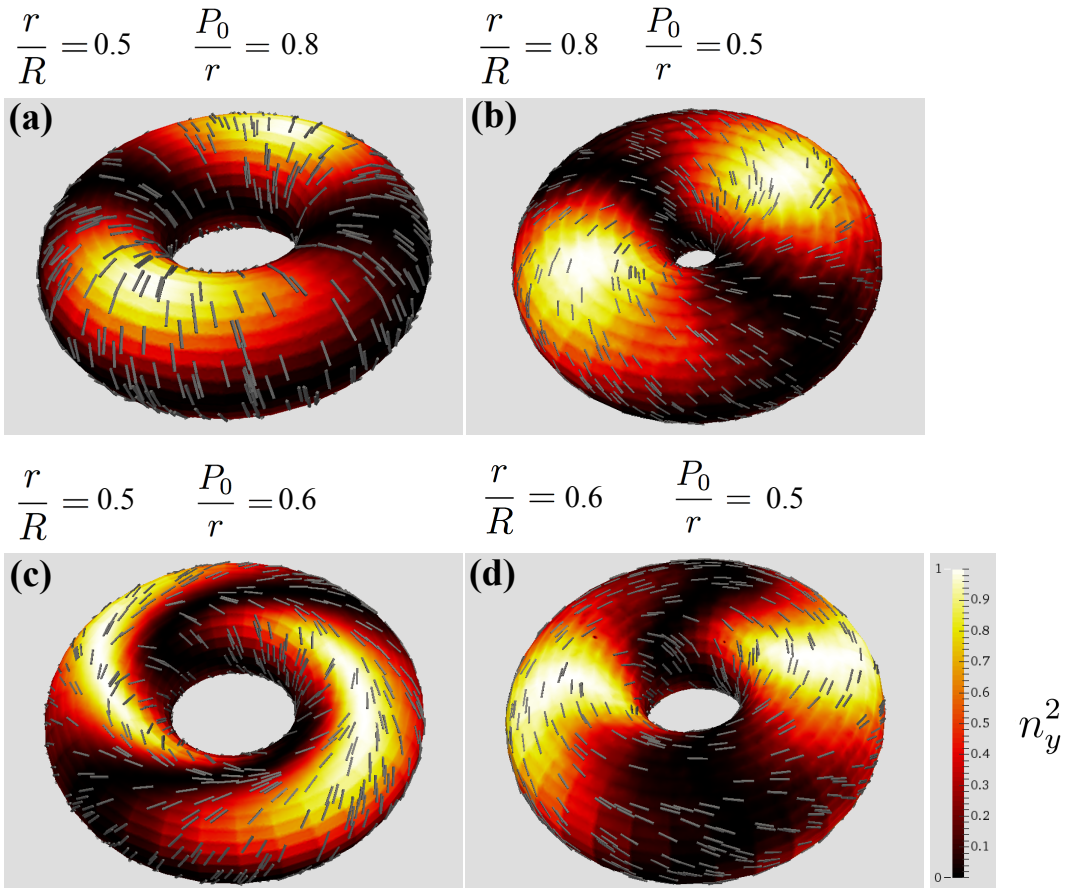

Figure 4.14: Orientation of the director field on the surface of a torus filled with cholesteric liquid crystal. (a) $\frac{r}{R}=0.5$, $\frac{P_0}{r}=0.8$, (b) $\frac{r}{R}=0.8$, $\frac{P_0}{r}=0.5$, (c) $\frac{r}{R}=0.6$, $\frac{P_0}{r}=0.5$, (d) $\frac{r}{R}=0.6$, $\frac{P_0}{r}=0.5$. The color scale refers to n_y^2 and the grey bars represent the director field.

Chapter 5

Conclusions

Nematics and cholesterics are known for their vast applications in photonics. After the great triumph of the flat display technology, researchers are interested in the role of complex confining geometries in the liquid crystal properties. As examples, there are the studies of spherical droplets and spherical shells, identified as possible building blocks for metamaterials with controllable optical properties. Applications range from bio-sensors to optical switches and privacy windows.

Because of the interplay with topology, curved surfaces are of special interest. When the liquid crystals are confined by curved surfaces, the topological constraints play a pivotal role in the configurations. In particular, for surfaces with Euler characteristic different from zero, the presence of topological defects is imposed. The material properties of the liquid crystals, the anchoring at the surface and the geometrical characteristics of the systems, all act as controlling parameters for the stability of the configurations.

In order to complement the investigation of the influence of topology in the physical properties of liquid crystals, it is important to study surfaces with geometries that are distinct from the spherical one. Recent experimental advances have allowed the production of liquid crystal droplets with handles, like the torus.

The torus has Euler characteristic equal to zero. Therefore, the configuration on the surface of the torus does not need to include topological defects. However, the curvature influences the configurations in a non-trivial way, as seen for nematic toroidal droplets where a chiral texture is observed. That is what distinguishes the torus from other curved systems, while being a highly complex structure with two different curvatures, its topology does not impose the presence of defects. This allows the study of the effects due solely to curvature and confinement.

In this thesis, we considered a toroidal droplet filled with cholesteric liquid crystal. The periodicity of the cholesteric defines an additional length scale, increasing the complexity of the system. We aimed at understanding how the ratio between the pitch of the cholesteric and the radii of the torus affects the configurations. Also, and from a more fundamental point of view, we wanted to understand how the confinement and curvature of the system will affect the intrinsic periodicity of the cholesteric.

We studied the equilibrium configurations obtained from the numerical minimization of the Landau-de Gennes free energy. In order to address the fundamental issue of the curvature effects on the cholesteric, we have developed the study in three stages.

First, we studied the equilibrium configurations of a cholesteric close to a curved wall. We find that, because of the curvature, the cholesteric is subjected to bend and splay distortions that influence the orientation field. As a result, the preferred local orientation is parallel to the symmetry axis of the system. This effect introduces changes in the periodicity of the cholesteric twist. The strength of the distortions depends on the curvature radius of the surface.

Then, we considered that the cholesteric was confined to a toroidal particle with imposed cylindrical symmetry. Inside the torus we find that the configurations are radially twisted, forming cholesteric layers along the radial direction. We compare these configurations with the ones formed inside an infinite cylinder, which corresponds to the limit with no curvature. We observe that, in the presence of curvature, there is a shift in the position of the cholesteric layers. This is a result of the periodicity distortions due to the curvature. The effect is more pronounced for smaller curvature radii. Other important factor is the commensurability between the pitch and the cross-sectional radius of the torus. When the two length scales commensurate, the configurations are more symmetric and stable.

Finally, we lifted the imposition of cylindrical symmetry. This allowed us to simulate more realistic systems and allowing the liquid crystal molecules to freely align at the boundary. With this kind of systems, we corroborate the results found for systems with cylindrical symmetry. The distortion of the natural periodicity depends heavily on the curvature of the droplet. However, because the system is less constrained, specially at the surface, we observe an increasing of the effect for non-commensurable geometries.

Our main conclusion is that the curvature of the toroidal shape affects the local orientation of the cholesteric molecules, distorting the twist inside the droplet. The result is a symmetry breaking of the cholesteric layers that depends mostly

on the curvature of the torus and on the commensurability between the pitch and geometrical parameters.

As an extension of this work, it would be of interest the study of droplets with multiple handles. Multiple handle bodies impose the existence of defects and would allow to investigate if the presence of defects has only a localized effect or if it will help accommodate the distortions imposed by the curvature. Also of interest is the elastic anisotropy and the inclusion of extra elastic deformations. For example, in cylinders, it has been found that the elastic properties are important parameters for the surface configuration. It would be interesting to understand how the second curvature would play a role for tori.

Appendix A

The Euler-Lagrange equations

We want to calculate the Euler-Lagrange equations that correspond to the Landau-de Gennes free energy for the independent components $q_i, i = 1, 2, 3, 4, 5$, of the order parameter tensor $\mathbf{Q}$.

The Euler-Lagrange equations are given by

$$\partial_i \left[\frac{\partial f}{\partial q_j} \right] - \frac{\partial f}{\partial q_j} = 0, \tag{A.1}$$

with the bulk free energy density

$$f = f_{ord} + f_{elas}, \tag{A.2}$$

$$f_{ord} = \frac{2}{3}\tau Q_{\alpha\beta}Q_{\beta\alpha} - \frac{8}{3}Q_{\alpha\beta}Q_{\beta\gamma}Q_{\gamma\alpha} + \frac{4}{9}\left(Q_{\alpha\beta}Q_{\beta\alpha}\right)^2 \tag{A.3}$$

$$\begin{aligned} f_{elas} &= \frac{1}{3+2\kappa}\left[Q_{\alpha\beta,\gamma}Q_{\alpha\beta,\gamma} + \kappa Q_{\alpha\beta,\beta}Q_{\alpha\gamma,\gamma} + 4q_0 Q_{\alpha\delta}\varepsilon_{\alpha\beta\gamma}Q_{\gamma\delta,\beta}\right. \\ &+ \left. 4q_0^2 Q_{\alpha\beta}Q_{\beta\alpha}\right] \end{aligned} \tag{A.4}$$

$Q_{\alpha\beta}$ designates the components of the order parameter tensor, $\varepsilon_{\alpha\beta\gamma}$ is the Levi-Civita tensor, $\tau = \frac{24AC}{B^2}$ is the dimensionless temperature, $\kappa = \frac{L_2}{L_1}$ is the reduced elastic constant, $q_0 = \frac{2\pi}{P}$ is the inverse cholesteric pitch, and $Q_{\alpha\beta,\gamma}$ designates the derivative $\frac{\partial Q_{\alpha\beta}}{\partial x_\gamma}$.

The equations have to be calculated under the constraints of symmetry $Q_{\alpha\beta} = Q_{\beta\alpha}$ and null trace $Q_{\alpha\alpha} = 0$ of the tensor $\mathbf{Q}$. These properties allow us to write the

tensor $\mathbf{Q}$ in its explicit form:

$$\mathbf{Q} = \begin{bmatrix} q_1 & q_2 & q_3 \\ q_2 & q_4 & q_5 \\ q_3 & q_5 & -(q_1+q_4) \end{bmatrix}. \tag{A.5}$$

We then express all the free energy density terms explicitly in terms of the independent components q_1, q_2, q_3, q_4 and q_5:

$$\begin{aligned}
Q_{\alpha\beta}Q_{\beta\alpha} &= Tr\left(Q^2\right) = 2\left(q_1^2+q_2^2+q_3^2+q_4^2+q_5^2+q_1q_4\right) && \text{(A.6)}\\
Q_{\alpha\beta}Q_{\beta\gamma}Q_{\gamma\alpha} &= Tr\left(Q^3\right) = -3\left[q_1^2q_4 - q_2^2\left(q_1+q_4\right)+q_3^2q_4+q_4^2q_1+q_5^2q_1\right. && \text{(A.7)}\\
&- \left. 2q_2q_3q_5\right]\\
Q_{\alpha\beta,\gamma}Q_{\alpha\beta,\gamma} &= 2\left[\left(\nabla q_1\right)^2+\left(\nabla q_2\right)^2+\left(\nabla q_3\right)^2+\left(\nabla q_4\right)^2+\left(\nabla q_5\right)^2+\nabla q_1\nabla q_4\right] && \text{(A.8)}\\
Q_{\alpha\beta,\beta}Q_{\alpha\gamma,\gamma} &= (q_{1,x})^2+(q_{2,x})^2+(q_{3,x})^2+(q_{2,y})^2+(q_{4,y})^2+(q_{5,y})^2+(q_{3,z})^2\\
&+ (q_{5,z})^2+(q_{1,z})^2+(q_{4,z})^2+2(q_{1,z})(q_{4,z})+2[(q_{1,x})(q_{2,y})\\
&+ (q_{2,x})(q_{4,y})+(q_{3,x})(q_{5,y})]+2[(q_{1,x})(q_{3,z})+(q_{2,x})(q_{5,z})\\
&- (q_{3,x})(q_{1,z})-(q_{3,x})(q_{4,z})]+2[(q_{2,y})(q_{3,z})+(q_{4,y})(q_{5,z}) && \text{(A.9)}\\
&- (q_{5,y})(q_{1,z})-(q_{5,y})(q_{4,z})]\\
Q_{\alpha\delta}\varepsilon_{\alpha\beta\gamma}Q_{\gamma\delta,\beta} &= q_1q_{3,y}+q_2q_{5,y}-q_3q_{1,y}-q_3q_{4,y}+q_2q_{1,z}+q_4q_{2,z}+q_5q_{3,z} && \text{(A.10)}\\
&+ q_3q_{2,x}+q_5q_{4,x}-q_1q_{5,x}-q_4q_{5,x}-q_1q_{2,z}-q_2q_{4,z}-q_3q_{5,z}\\
&- q_2q_{3,x}-q_4q_{5,x}+q_5q_{1,x}+q_5q_{4,x}-q_3q_{1,y}-q_5q_{2,y}+q_1q_{3,y}+q_4q_{3,y}
\end{aligned}$$

From the definition (A.1), we can now calculate the Euler-Lagrange equations in this explicit form. In this thesis we have assumed the one-elastic constant approximation, $\kappa = 0$. The 5 equations obtained are:

$$-\nabla^2 q_1 - 2q_0\left[q_{2,z}-q_{3,y}\right]+2q_0\left[-q_{2,z}+q_{3,y}\right] = -\omega\left[\Sigma q_1 - 6A_{11}+2TrQ^2\right] \tag{A.11}$$

$$\begin{aligned}
-\nabla^2 q_2 - q_0\left[-q_{1,z}+q_{3,x}+q_{4,z}-q_{5,y}\right]+q_0\left[q_{1,z}-q_{3,x}-q_{4,z}+q_{5,y}\right] = && \text{(A.12)}\\
= -\omega\left[\Sigma q_2 - 6A_{12}\right]
\end{aligned}$$

$$\begin{aligned}
-\nabla^2 q_3 - q_0\left[2q_{1,y}-q_{2,x}+q_{4,y}+q_{5,z}\right]+q_0\left[-2q_{1,y}+q_{2,x}-q_{4,y}-q_{5,z}\right] = && \text{(A.13)}\\
= -\omega\left[\Sigma q_3 - 6A_{13}\right]
\end{aligned}$$

$$-\nabla^2 q_4 - 2q_0\left[-q_{2,z}+q_{5,x}\right]+2q_0\left[q_{2,z}-q_{5,x}\right] = -\omega\left[\Sigma q_4 - 6A_{22}+2TrQ^2\right] \tag{A.14}$$

$$-\nabla^2 q_5 - q_0\left[-q_{1,x} + q_{2,y} - q_{3,z} - 2q_{4,x}\right] + q_0\left[q_{1,x} - q_{2,y} + q_{3,z} + 2q_{4,x}\right] = \quad \text{(A.15)}$$
$$= -\omega\left[\Sigma q_5 - 6A_{23}\right]$$

with the definitions

$$\omega = \frac{6+4\kappa}{3} = 2 \quad \text{(A.16)}$$

$$\Sigma = \tau + \frac{4}{3}TrQ^2 + \frac{6}{3+2\kappa}q_0^2 = \tau + \frac{4}{3}TrQ^2 + 2q_0^2 \quad \text{(A.17)}$$

$$A_{11} = q_1^2 + q_2^2 + q_3^2 \quad \text{(A.18)}$$

$$A_{12} = q_1 q_2 + q_2 q_4 + q_3 q_5 \quad \text{(A.19)}$$

$$A_{13} = q_2 q_5 - q_3 q_4 \quad \text{(A.20)}$$

$$A_{22} = q_2^2 + q_4^2 + q_5^2 \quad \text{(A.21)}$$

$$A_{23} = q_2 q_3 - q_5 q_1 \quad \text{(A.22)}$$

The second and third terms in the left-hand side of Eqs. (A.11 - A.15) are deliberately kept apart, even though they are equal. This is because the term that originates from $\partial_i\left[\frac{\partial f}{\partial q_j}\right]$ contributes to the surface. The two terms must, therefore, be entered separately in the COMSOL numeric model.

Appendix B

Euler-Lagrange equations with cylindrical symmetry

In order to impose cylindrical symmetry around the z axis, we start by writing the Euler-Lagrange equations in cylindrical coordinates (ρ, θ, z). In cylindrical coordinates, the Euler Lagrange equations for the Landau-de Gennes free energy are:

$$\begin{aligned} &- \left(\frac{\partial^2 q_1}{\partial \rho^2} + \frac{1}{\rho}\frac{\partial q_1}{\partial \rho} + \frac{1}{\rho^2}\frac{\partial^2 q_1}{\partial \theta^2} + \frac{\partial^2 q_1}{\partial z^2}\right) - 2q_0\left(\frac{\partial q_2}{\partial z} - \sin\theta\frac{\partial q_3}{\partial \rho}\right. \\ &- \left.\frac{\cos\theta}{\rho}\frac{\partial q_3}{\partial \theta}\right) + 2q_0\left(-\frac{\partial q_2}{\partial z} + \sin\theta\frac{\partial q_3}{\partial \rho} + \frac{\cos\theta}{\rho}\frac{\partial q_3}{\partial \theta}\right) = -\omega\left[\Sigma q_1 - 6A_{11}\right. \\ &+ \left. 2TrQ^2\right] \end{aligned} \tag{B.1}$$

$$\begin{aligned} &- \left(\frac{\partial^2 q_2}{\partial \rho^2} + \frac{1}{\rho}\frac{\partial q_2}{\partial \rho} + \frac{1}{\rho^2}\frac{\partial^2 q_2}{\partial \theta^2} + \frac{\partial^2 q_2}{\partial z^2}\right) - q_0\left(-\frac{\partial q_1}{\partial z} + \cos\theta\frac{\partial q_3}{\partial \rho} - \frac{\sin\theta}{\rho}\frac{\partial q_3}{\partial \theta}\right. \\ &+ \left.\frac{\partial q_4}{\partial z} - \sin\theta\frac{\partial q_5}{\partial \rho} - \frac{\cos\theta}{\rho}\frac{\partial q_5}{\partial \theta}\right) + q_0\left(\frac{\partial q_1}{\partial z} - \cos\theta\frac{\partial q_3}{\partial \rho} + \frac{\sin\theta}{\rho}\frac{\partial q_3}{\partial \theta} - \frac{\partial q_4}{\partial z}\right. \\ &+ \left.\sin\theta\frac{\partial q_5}{\partial \rho} + \frac{\cos\theta}{\rho}\frac{\partial q_5}{\partial \theta}\right) = -\omega\left[\Sigma q_2 - 6A_{12}\right] \end{aligned} \tag{B.2}$$

$$\begin{aligned} &- \left(\frac{\partial^2 q_3}{\partial \rho^2} + \frac{1}{\rho}\frac{\partial q_3}{\partial \rho} + \frac{1}{\rho^2}\frac{\partial^2 q_3}{\partial \theta^2} + \frac{\partial^2 q_3}{\partial z^2}\right) - q_0\left(2\sin\theta\frac{\partial q_1}{\partial \rho} + 2\frac{\cos\theta}{\rho}\frac{\partial q_1}{\partial \theta} - \cos\theta\frac{\partial q_2}{\partial \rho}\right. \\ &+ \left.\frac{\sin\theta}{\rho}\frac{\partial q_2}{\partial \theta} + \sin\theta\frac{\partial q_4}{\partial \rho} + \frac{\cos\theta}{\rho}\frac{\partial q_4}{\partial \theta} + \frac{\partial q_5}{\partial z}\right) + q_0\left(-2\sin\theta\frac{\partial q_1}{\partial \rho} - 2\frac{\cos\theta}{\rho}\frac{\partial q_1}{\partial \theta} + \cos\theta\frac{\partial q_2}{\partial \rho}\right. \\ &- \left.\frac{\sin\theta}{\rho}\frac{\partial q_2}{\partial \theta} - \sin\theta\frac{\partial q_4}{\partial \rho} - \frac{\cos\theta}{\rho}\frac{\partial q_4}{\partial \theta} - \frac{\partial q_5}{\partial z}\right) = -\omega\left[\Sigma q_3 - 6A_{13}\right] \end{aligned} \tag{B.3}$$

$$
\begin{aligned}
- & \left(\frac{\partial^2 q_4}{\partial\rho^2}+\frac{1}{\rho}\frac{\partial q_4}{\partial\rho}+\frac{1}{\rho^2}\frac{\partial^2 q_4}{\partial\theta^2}+\frac{\partial^2 q_4}{\partial z^2}\right)-2q_0\left(-\frac{\partial q_2}{\partial z}+\cos\theta\frac{\partial q_5}{\partial\rho}\right. \\
- & \left.\frac{\sin\theta}{\rho}\frac{\partial q_5}{\partial\theta}\right)+2q_0\left(\frac{\partial q_2}{\partial z}-\cos\theta\frac{\partial q_5}{\partial\rho}+\frac{\sin\theta}{\rho}\frac{\partial q_5}{\partial\theta}\right)=-\omega\left[\Sigma q_4-6A_{22}\right. \\
+ & \left.2TrQ^2\right]
\end{aligned}
\tag{B.4}
$$

$$
\begin{aligned}
- & \left(\frac{\partial^2 q_5}{\partial\rho^2}+\frac{1}{\rho}\frac{\partial q_5}{\partial\rho}+\frac{1}{\rho^2}\frac{\partial^2 q_5}{\partial\theta^2}+\frac{\partial^2 q_5}{\partial z^2}\right)-q_0\left(-\cos\theta\frac{\partial q_1}{\partial\rho}+\frac{\sin\theta}{\rho}\frac{\partial q_1}{\partial\theta}+\sin\theta\frac{\partial q_2}{\partial\rho}\right. \\
+ & \left.\frac{\cos\theta}{\rho}\frac{\partial q_2}{\partial\theta}-\frac{\partial q_3}{\partial z}-2\cos\theta\frac{\partial q_4}{\partial\rho}+\frac{2\sin\theta}{\rho}\frac{\partial q_4}{\partial\theta}\right)+q_0\left(\cos\theta\frac{\partial q_1}{\partial\rho}-\frac{\sin\theta}{\rho}\frac{\partial q_1}{\partial\theta}-\sin\theta\frac{\partial q_2}{\partial\rho}\right. \\
- & \left.\frac{\cos\theta}{\rho}\frac{\partial q_2}{\partial\theta}+\frac{\partial q_3}{\partial z}+2\cos\theta\frac{\partial q_4}{\partial\rho}-\frac{2\sin\theta}{\rho}\frac{\partial q_4}{\partial\theta}\right)=-\omega\left[\Sigma q_5-6A_{23}\right]
\end{aligned}
\tag{B.5}
$$

For systems with cylindrical symmetry, we can simulate just a cross-section, corresponding to a fixed value of θ. Therefore, we eliminate the variable θ from the equations. Unlike what happens for an infinite system, the derivatives in θ are not zero. Their expression can be obtained by imposing the cylindrical symmetry.

If a liquid crystal system has cylindrical symmetry around the z-axis, then the order parameter for any value of the orientation θ, $Q_{\alpha\beta}(\rho,\theta,z)$ is obtained from $Q_{\gamma\delta}(\rho,\theta=0,z)$ by a rotation operation

$$
Q_{\alpha\beta}(\rho,\theta,z)=T_{\alpha\gamma}(\theta)Q_{\gamma\delta}(\rho,\theta=0,z)T^{\dagger}_{\delta\beta}(\theta), \tag{B.6}
$$

$$
T_{\alpha\beta}=\begin{bmatrix}\cos\theta & -\sin\theta & 0\\ \sin\theta & \cos\theta & 0\\ 0 & 0 & 1\end{bmatrix}. \tag{B.7}
$$

The dependence in the variable θ comes exclusively from the transformation matrix $T_{\alpha\beta}$. Having the order parameter $Q_{\alpha\beta}(\rho,\theta,z)$ expressed in this way, one can calculate its derivatives in order to θ [46]. In particular, for $\theta=0$, we have

$$
\frac{\partial Q_{\alpha\beta}}{\partial\theta}(\rho,\theta=0,z)=\begin{bmatrix}-2q_2 & (q_1-q_4) & -q_5\\ (q_1-q_4) & 2q_2 & q_3\\ -q_5 & q_3 & 0\end{bmatrix} \tag{B.8}
$$

and

$$
\frac{\partial^2 Q_{\alpha\beta}}{\partial\theta^2}(\rho,\theta=0,z)=\begin{bmatrix}2(q_4-q_1) & -4q_2 & -q_3\\ -4q_2 & 2(q_1-q_4) & -q_5\\ -q_3 & -q_5 & 0\end{bmatrix}. \tag{B.9}
$$

Substituting the θ dependance for the particular case $\theta = 0$ into the Eqs (B.1 - B.5), we get to the final form of the Euler-Lagrange equations with imposed cylindrical symmetry.

$$\begin{aligned} - & \left(\frac{\partial^2 q_1}{\partial \rho^2} + \frac{\partial^2 q_1}{\partial z^2}\right) - \left[\frac{1}{\rho}\frac{\partial q_1}{\partial \rho} + 2q_0\frac{\partial q_2}{\partial z}\right] + 2q_0\left[-\frac{\partial q_2}{\partial z}\right] \\ = & -\omega\left[\Sigma q_1 - 6A_{11} + 2TrQ^2\right] + \frac{2}{\rho^2}\left(q_4 - q_1\right) + \frac{4}{\rho}q_0 q_5 \end{aligned} \tag{B.10}$$

$$\begin{aligned} - & \left(\frac{\partial^2 q_2}{\partial \rho^2} + \frac{\partial^2 q_2}{\partial z^2}\right) - \left[\frac{1}{\rho}\frac{\partial q_2}{\partial \rho} + q_0\left(-\frac{\partial q_1}{\partial z} + \frac{\partial q_3}{\partial \rho} + \frac{\partial q_4}{\partial z}\right)\right] \\ + & q_0\left[\frac{\partial q_1}{\partial z} - \frac{\partial q_3}{\partial \rho} - \frac{\partial q_4}{\partial z}\right] = -\omega\left[\Sigma q_2 - 6A_{12}\right] - \frac{4}{\rho^2}q_2 - \frac{2}{\rho}q_0 q_3 \end{aligned} \tag{B.11}$$

$$\begin{aligned} - & \left(\frac{\partial^2 q_3}{\partial \rho^2} + \frac{\partial^2 q_3}{\partial z^2}\right) - \left[\frac{1}{\rho}\frac{\partial q_3}{\partial \rho} + q_0\left(-\frac{\partial q_2}{\partial \rho} + \frac{\partial q_5}{\partial z}\right)\right] \\ + & q_0\left[\frac{\partial q_2}{\partial \rho} - \frac{\partial q_5}{\partial z}\right] = -\omega\left[\Sigma q_3 - 6A_{13}\right] - \frac{1}{\rho^2}q_3 - \frac{4}{\rho}q_0 q_2 \end{aligned} \tag{B.12}$$

$$\begin{aligned} - & \left(\frac{\partial^2 q_4}{\partial \rho^2} + \frac{\partial^2 q_4}{\partial z^2}\right) - \left[\frac{1}{\rho}\frac{\partial q_4}{\partial \rho} + 2q_0\left(-\frac{\partial q_2}{\partial z} + \frac{\partial q_5}{\partial \rho}\right)\right] + 2q_0\left[\frac{\partial q_2}{\partial z}\right. \\ - & \left.\frac{\partial q_5}{\partial \rho}\right] = -\omega\left[\Sigma q_4 - 6A_{22} + 2TrQ^2\right] + \frac{2}{\rho^2}\left(q_1 - q_4\right) \end{aligned} \tag{B.13}$$

$$\begin{aligned} - & \left(\frac{\partial^2 q_5}{\partial \rho^2} + \frac{\partial^2 q_5}{\partial z^2}\right) - \left[\frac{1}{\rho}\frac{\partial q_5}{\partial \rho} + q_0\left(-\frac{\partial q_1}{\partial \rho} - \frac{\partial q_3}{\partial z} - 2\frac{\partial q_4}{\partial \rho}\right)\right] \\ + & q_0\left[\frac{\partial q_1}{\partial \rho} + \frac{\partial q_3}{\partial z} + 2\frac{\partial q_4}{\partial \rho}\right] = -\omega\left[\Sigma q_5 - 6A_{23}\right] - \frac{1}{\rho^2}q_5 + \frac{2}{\rho}q_0\left(q_1 - q_4\right) \end{aligned} \tag{B.14}$$

Appendix C

The twist parameter

One can characterize the twisted configurations by a twist parameter which is constructed using the chiral term in the free energy, without the unnecessary multiplicative constant [52]:

$$S_{tw} = \varepsilon_{ikl} Q_{ij} \frac{\partial Q_{lj}}{\partial x_k}, \tag{C.1}$$

with ε_{ikl} being the Levi-Civita tensor, Q_{ij} the components of the order parameter tensor $\mathbf{Q}$, and $x_k = x, y, z$ the cartesian coordinates.

The twist parameter defined in Eq.C.1 is a measure of the local amount of twist in the system and it is therefore the adequate quantity to probe spatial variations of the pitch. To better understand the meaning of this parameter, let us consider the following ansatz for a cholesteric configuration with single twist perpendicular to the z direction:

$$\mathbf{n} = (\cos(q_0 z), \sin(q_0 z), 0)\,, \tag{C.2}$$

where q_0 is the inverse cholesteric pitch $q_0 = \frac{2\pi}{P_0}$.

Using the definition of the $\mathbf{Q}$-tensor order parameter for uniaxial liquid crystal, $Q_{\alpha\beta} = \frac{S}{2}(3n_\alpha n_\beta - \delta_{\alpha\beta})$, where S is the scalar bulk order parameter and calculating S_{tw}, we reach the result:

$$S_{tw} = -\frac{9S^2}{4} q_0. \tag{C.3}$$

The minus sign is a result of the ansatz having twist in the anti-clockwise direction, while the definition of S_{tw} yields a positive value for the clockwise direction. We can see that the twist parameter is proportional to the inverse pitch, with a proportionality constant that depends on a numeric factor and on the square of the scalar order parameter.

In order to calculate this parameter, it is useful to express S_{tw} explicitly in terms

of the 5 independent components q_i, $i = 1, 2, 3, 4, 5$ of the **Q**-tensor.

$$\begin{aligned} S_{tw} &= q_1\left(-q_{2,z} + 2q_{3,y} - q_{5,x}\right) \\ &+ q_2\left(q_{1,z} - q_{3,x} - q_{4,z} + q_{5,y}\right) \\ &+ q_3\left(-2q_{1,y} + q_{2,x} - q_{4,y} - q_{5,z}\right) \\ &+ q_4\left(q_{2,z} + q_{3,y} - 2q_{5,x}\right) \\ &+ q_5\left(q_{1,x} - q_{2,y} + q_{3,z} + 2q_{4,x}\right) \end{aligned} \tag{C.4}$$

$q_{i,k}$ designates the derivative $\frac{\partial q_i}{\partial x_k}$.

A simple rearrangement of the twist parameter S_{tw} gives us an expression for the cholesteric pitch $P = -\frac{9\pi}{2}\frac{S^2}{S_{tw}}$. We are interested in analyzing how the measured pitch deviates from the natural pitch P_0, which can be obtained by

$$\frac{P}{P_0} = -\frac{9S^2}{4}\frac{q_0}{S_{tw}}. \tag{C.5}$$

Bibliography

[1] Timothy J. Sluckin, David A. Dunmur, and Horst Stegemeyer. *Crystals that Flow: Classic papers from the history of liquid crystals*. Taylor and Francis, 2004.

[2] Nobel Media. Liquid crystals. `http://www.nobelprize.org/educational/physics/liquid_crystals/history`, 2014.

[3] Peter J. Collings. *Liquid Crystals, Nature's Delicate Phase of Matter*. Princeton University Press, 1990.

[4] Peter J. Collings and Michael Hird. *Introduction to Liquid Crystals, Chemistry and Physics*. Taylor and Francis, 1997.

[5] P. G. de Gennes and J. Prost. *The Physics of Liquid Crystals*. Oxford University Press, 1993.

[6] Derek Gray. Introduction to liquid crystals. `http://barrett-group.mcgill.ca/tutorials/liquid_crystal/LC01.htm`.

[7] P. M. Chaikin and T. C. Lubensky. *Princinples of condensed matter physics*. Cambridge University Press, 1995.

[8] Cyril Hilsum. Flat-panel electronic displays: a triumph of physics, chemistry and engineering. *Phil. Trans. R. Soc. A*, 368:1027–1082, 2010.

[9] Stefan Agamanolis. Liquid crystal displays: Past, present, and future. `http://web.media.mit.edu/~stefan/liquid-crystals/liquid-crystals.html`, 1995.

[10] Displaysearch: Lcd industry poised for recovery in 2012. `http://electroiq.com/blog/2012/09/displaysearch-lcd-industry-poised-for-recovery-in-2012/`, September 2012.

[11] Yiqun Bai and Nicholas L. Abbott. Recent advances in colloidal and interfacial phenomena involving liquid crystals. *Langmuir*, 27:5719–5738, 2011.

[12] Sri Sivakumar, Kim L. Wark, Jugal K. Gupta, Nicholas L. Abbott, and Frank Caruso. Liquid crystal emulsions as the basis of biological sensors for the optical detection of bacteria and viruses. *Advanced Functional Materials*, 19(14):2260–2265, 2009.

[13] Gaetano Napoli and Luigi Vergori. Extrinsic curvature effects on nematic shells. *Phys. Rev. Lett.*, 108:207803, 2012.

[14] N. D. Mermin. The topological theory of defects in ordered media. *Rev. Mod. Phys.*, 51(3):591–648, 1979.

[15] David R. Nelson. Toward a tetravalent chemistry of colloids. *Nano Letters*, 2(10):1125–1129, 2002.

[16] Devries G. A., Brunnbauer M., Hu Y., Jackson A. M., Long B., Neltner B. T., Uzun O., Wunsch B. H., and Stellacci F. Divalent metal nanoparticles. *Science*, 315:358–361, 2007.

[17] Leonid V. Mirantsev, Andre M. Sonnet, and Epifanio G. Virga. Geodesic defect anchoring on nematic shells. *Phys. Rev. E*, 86:020703, 2012.

[18] Teresa Lopez-Leon and Alberto Fernandez-Nieves. Drops and shells of liquid crystal. *Colloid. Polym. Sci.*, 289:345–359, 2011.

[19] T. Lopez-Leon, V. Koning, K. B. S. Devaiah, V. Vitelli, and A. Fernandez-Nieves. Frustrated nematic order in spherical geometries. *Nature Physics*, 7:391–394, 2011.

[20] Tereza Lopez-Leon, Martin A. Bates, and Alberto Fernández-Nieves. Defect coalescence in spherical nematic shells. *Phys. Rev. E*, 86:030702(R), 2012.

[21] T. Lopez-Leon and A. Fernandez-Nieves. Topological transformations in bipolar shells of nematic liquid crystals. *Phys. Rev. E*, 79:021707, 2009.

[22] V. Vitelli and D. R. Nelson. Nematic textures in spherical shells. *Phys. Rev. E*, 74:021711, 2006.

[23] A. Fernandez-Nieves, V. Vitelli, A. S. Utada, D. R. Link, M. Marquez, D. R. Nelson, and D. A. Weitz. Novel defect structures in nematic liquid crystal shells. *Phys. Rev. Lett.*, 99:157801, 2007.

[24] David Sec, Teresa Lopez-Leon, Maurizio Nobili, Christophe Blanc, Alberto Fernandez-Nieves, Miha Ravnik, and Slobodan Zumer. Defect trajectories in nematic shells: Role of elastic anisotropy and thickness heterogeneity. *Phys. Rev. E*, 86:020705(R), 2012.

[25] Vinzenz Koning, Teresa Lopez-Leon, Alberto Fernandez-Nieves, and Vincenzo Vitelli. Bivalent defect configurations in inhomogeneous nematic shells. *Soft Matter*, 9:4993–5003, 2013.

[26] E. Pairam and A. Fernández-Nieves. Generation and stability of toroidal droplets in a viscous liquid. *Phys. Rev. Lett.*, 102:234501, 2009.

[27] Ekapop Pairam, Jayalakshmi Vallamkondu, and Alberto Fernández-Nieves. Nematic order of handle droplets. `http://fernandezlab.gatech.edu/research/Ekapop2013/Ekapop.html`, 2013.

[28] Antonio Segatti, Michael Snarski, and Marco Veneroni. Equilibrium configurations of nematic liquid crystals on a torus. *Phys. Rev. E*, 90:012501, 2014.

[29] Vinzenz Koning, Benjamin C. van Zuiden, Randall D. Kamien, , and Vincenzo Vitelli. Saddle-splay screening and chiral symmetry breaking in toroidal nematics. *Soft matter*, 10(23):4192–4198, 2014.

[30] Ekapop Pairam, Jayalakshmi Vallamkondu, Vinzenz Koning, Benjamin C. van Zuiden, Perry W. Ellis, Martin A. Bates, Vincenzo Vitelli, and Alberto Fernandez-Nieves. Stable nematic droplets with handles. *PNAS*, 110(23):9295–9300, 2013.

[31] M. Ambrozic and S. Zumer. Chiral nematic liquid crystals in cylindrical cavities. *Phys. Rev. E*, 54(5):5187–5197, 1996.

[32] M. Ambrozic and S. Zumer. Axially twisted chiral nematic structures in cylindrical cavitie. *Phys. Rev. E*, 59(4):4153–4160, 1999.

[33] F. Xu and P. P. Crooker. Chiral nematic droplets with parallel surface anchoring. *Phys. Rev. E*, 56(6):6853–6860, 1997.

[34] David Sec, Tine Porenta, Miha Ravnik, and Slobodan Zumer. Geometrical frustration of chiral ordering in cholesteric droplets. *Soft Matter*, xx:1–8, 2012.

[35] D. Andrienko, M. Tasinkevych, P. Patrício, and M. M. Telo da Gama. Interaction of colloids with a nematic-isotropic interface. *Phys. Rev. E*, 69:021706, 2004.

[36] N. M. Silvestre, Z. Eskandari, P. Patrício, J. M. Romero-Enrique, and M. M. Telo da Gama. Nematic wetting and filling of crenellated surfaces. *Phys. Rev. E*, 89:011703, 2012.

[37] G. Vertogen and W. H. de Jeu. *Thermotropic Liquid Crystals, Fundamentals.* Springer-Verlag Berlin, 1988.

[38] G. Barbero and G. Durand. Splay-bend curvature and temperature-induced surface transitions in nematic liquid crystals. *Phys. Rev. E*, 48(3):1942–1947, 1993.

[39] G. P. Crawford, D. W. Allender, and J. W. Doane. Surface elastic and molecular-anchoring properties of nematic liquid crystals confined to cylindrical cavities. *Phys. Rev. A*, 45(12):8693–8708, 1992.

[40] C. Blanc, D. Svensek, S. Zumer, and M. Nobili. Dynamics of nematic liquid crystal disclinations: The role of the backflow. *Phys. Rev. Lett.*, 95:097802, 2005.

[41] M. Nobili and G. Durand. Disorientation-induced disordering at a nematic-liquid-crystal-solid interface. *Phys. Rev. A*, 46:R6174(R), 1992.

[42] J.-B. Fournier and P. Galatola. Modeling planar degenerate wetting and anchoring in nematic liquid crystals. *Europhys. Lett.*, 72(3):403–409, 2005.

[43] R. D. Kamien. The geometry of soft materials: A primer. *Rev. Mod. Phys.*, 74(4):953–971, 2002.

[44] COMSOL, Inc., Burlington, MA. *COMSOL Multiphysics^{TM}, Version 3.2 User's Guide*, 2005. References therein `http://www.comsol.com`.

[45] N. M. Silvestre M. Tasinkevych and M. M. Telo da Gama. Liquid crystal boojum-colloids. *New J. Phys.*, 14:073030 (33pp), 2012.

[46] Jun ichi Fukuda, Makoto Yoneya, and Hiroshi Yokoyama. Nematic liquid crystal around a spherical particle: Investigation of the defect structure and its stability using adaptive mesh refinement. *Eur. Phys. J. E*, 13(1):87–98, 2004.

[47] Hang Si. Tetgen: A quality tetrahedral mesh generator and a 3d delaunay triangulator. `http://wias-berlin.de/software/tetgen/`, 2015.

[48] R. Cools. An encyclopaedia of cubature formulas. *J. Complexity*, 19:445–453, 2003.

[49] J.Ch. Gilbert and C. Lemaréchal. Some numerical experiments with variable-storage quasi-newton algorithms. *Mathematical Programming*, 45:407–435, 1989.

[50] Jorge Nocedal. Updating quasi-newton matrices with limited storage. *Math. Comp.*, 35:773–782, 1980.

[51] Utkarsh Ayachit. *The ParaView Guide: A Parallel Visualization Application*. Kitware, 2015. ISBN 978-1930934306.

[52] A. Kilian and A. Sonnet. On the analysis of twisted director configurations. *Z. Naturforsch. A*, 50(11):991–994, 1995.